PR12-14-002

Precision Measurements and Studies of a Possible Nuclear Dependence of $R = \sigma_L/\sigma_T$

S. Covrig, R. Ent, H. Fenker, D. Gaskell (spokesperson), D. Higinbotham, M. Jones, C. Keppel (spokesperson), S. P. Malace (contact and spokesperson), B. Sawatzky, and S. Wood
Thomas Jefferson National Accelerator Facility, Newport News, VA 23606, USA

A. Accardi, M. E. Christy (spokesperson), J. Diefenbach, P. Gueye, Y. Han, N. Kalantarians, M. Kohl, P. Monaghan, L. Tang, and L. Y. Zhu
Hampton University, Hampton, VA 23668, USA

V. Mamyan
Carnegie Mellon University, Pittsburgh, PA 15213, USA

W. Boeglin, P. E. C. Markowitz, and J. Reinhold
Florida International University, Miami, FL 33199, USA

G. Niculescu and I. Niculescu
James Madison University, Harrisonburg, VA 22807, USA

X. Jiang and J. Huang
Los Alamos National Laboratory, Los Alamos, NM 87544, USA

V. Sulkosky
Massachusetts Institute of Technology, Cambridge, MA 02139, USA

J. Dunne, D. Dutta
Mississippi State University, Mississippi State, MS 39762, USA

A. Daniel
University of Houston, Houston, TX 77004, USA

T. Badman, S. Li, E. Long, P. Solvignon (spokesperson), K. Slifer, and R. Zielinski
University of New Hampshire, Durham, NH 03824, USA

Z. Ahmed, G. Huber, and W. Li
University of Regina, Regina, SK S4S0A2, Canada

A. Bodek
University of Rochester, Rochester, NY 14627, USA

D. Hornidge
Mount Allison University, Sackville, NB, Canada

D. Day, D. Keller, O. Rondon, Z. Ye, and M. Yurov
University of Virginia, Charlottesville, VA 22904, USA

A. Asaturyan, A. Mkrtchyan, H. Mkrtchyan, V. Tadevosyan, and S. Zhamkochyan
I. A. Alikhanian National Science Laboratory (Yerevan Physics Institute), Yerevan, Armenia

V. Guzey
National Research Center "Kurchatov Institute", Petersburg Nuclear Physics Institute, Gatchina, 188300, Russia

A. Ahmidouch, S. Danagoulian
North Carolina AT State University, Greensboro, NC 27411, USA

F.R. Wasselmann
Xavier University of Louisiana, New Orleans, LA 70125, USA

L. Weinstein
Old Dominion University, Norfolk, VA 23529, USA

D. Androic
Faculty of Science, University of Zagreb Bijenicka 32, HR-10000 Zagreb

We propose to measure with unprecedented statistical precision inclusive inelastic electron-nucleon and electron-nucleus scattering cross sections in the DIS regime spanning a four-momentum transfer range of $1 < Q^2 < 5\ GeV^2$, and a Bjorken x range of $0.1 < x < 0.6$ for W^2 up to 10 GeV^2 using hydrogen, deuterium, carbon, copper, and gold targets. The cross sections will be used to perform high-precision Rosenbluth separations to extract the ratio $R = \sigma_L/\sigma_T$, $R_d - R_p$, $R_A - R_D$, and the transverse F_1, longitudinal F_L, and F_2 structure functions in a model-independent fashion. Recent analyses suggest that $R_A - R_D$ may be different than zero, having profound implications for our understanding of the origins of both antishadowing and the nuclear EMC effect. We request 22 days to set the most precise limit to date on the possible nuclear modifications of R.

I. BRIEF INTRODUCTION OF FORMALISM

Charged lepton–nucleon deep inelastic scattering (DIS) is a very powerful tool for studying the structure of the nucleon. The electromagnetic interaction governs the coupling of the charged lepton to the nucleon via exchange of virtual photons. In Quantum Electrodynamics, the charged lepton–virtual photon vertex is exactly calculable. The coupling of the virtual photon to the nucleon is described by the hadronic tensor which depends on two structure functions. The experimental mapping of these functions in a wide kinematic range and their description in a consistent theoretical model are aimed at understanding the makeup of the nucleon as seen by the electromagnetic probe.

In the one-photon exchange approximation, the cross section for charged lepton–nucleon scattering can be written as:

$$\frac{d^2\sigma}{d\Omega dE'} = \frac{\alpha^2}{Q^4}\frac{E'}{E}L_{\mu\nu}W^{\mu\nu} = \frac{4\alpha^2(E')^2}{Q^4}\cos^2\frac{\theta}{2} \times \left(\frac{F_2(x,Q^2)}{\nu} + \frac{2F_1(x,Q^2)}{M}\tan^2\frac{\theta}{2}\right), \tag{1}$$

where α is the fine structure constant, $Q^2 = 4EE' sin^2(\theta/2)$ is the four-momentum transfer squared, E and E' are the initial and scattered charged lepton energies, $L_{\mu\nu}$ and $W^{\mu\nu}$ are the leptonic and hadronic tensors, $\nu = E - E'$ is the energy transfer, $x = \frac{Q^2}{2M\nu}$ is the Bjorken scaling variable, θ is the detected lepton scattering angle while M is the nucleon mass. The dimensionless structure functions F_1 and F_2 reflect the probability of photo-absorption of either transversely (helicity $\pm$ 1) or longitudinally (helicity 0) polarized virtual photons.

In the quark–parton model the structure functions F_1 and F_2 are expressed in terms of the quark and anti-quark distribution functions as:

$$F_2(x) = 2xF_1 = x\sum_q e_q^2(q(x) + \bar{q}(x)), \tag{2}$$

where $q(x)$ is the probability to find inside the nucleon a quark of flavor q carrying a fraction x of the nucleon momentum. Beyond the quark-parton model the Q^2 dependence of the structure functions arises from perturbative Quantum Chromodynamics radiative effects as well as from non-perturbative $1/Q^2$ power corrections.

In the context of experimental observables, the cross section can be expressed in terms of the absorption cross sections of purely longitudinal (σ_L) or transverse (σ_T) photons as:

$$\frac{d^2\sigma}{d\Omega dE'} = \Gamma\left(\sigma_T(x,Q^2) + \epsilon\sigma_L(x,Q^2)\right) = \Gamma\sigma_T(1+\epsilon R), \tag{3}$$

with $R = \sigma_L/\sigma_T$, the flux of transverse virtual photons

$$\Gamma = \frac{\alpha}{2\pi^2 Q^2}\frac{E'}{E}\frac{K}{1-\epsilon}, K = \nu(1-x) \tag{4}$$

and the ratio of the longitudinal to transverse virtual photon polarizations

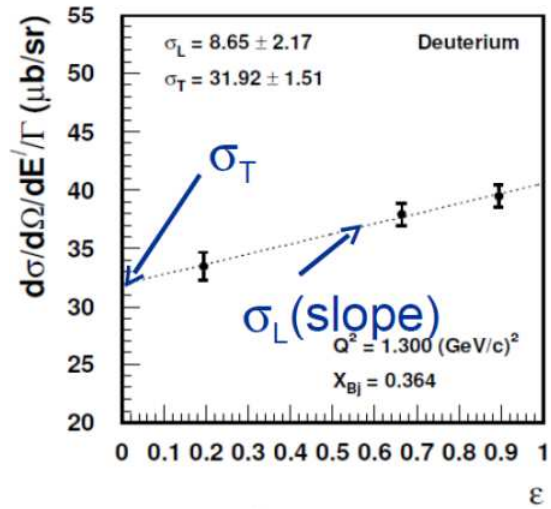

FIG. 1: An example of a L/T separation on a deuterium target using the Rosenbluth technique.

$$\epsilon = \left[1 + 2\left(1 + \frac{\nu^2}{Q^2}\right)\tan^2\frac{\theta}{2}\right]^{-1}. \tag{5}$$

The structure functions can then be written in terms of the virtual photon cross sections as:

$$F_1(x, Q^2) = \frac{KM}{4\pi^2\alpha}\sigma_T(x, Q^2), \tag{6}$$

$$F_L(x, Q^2) = \frac{2xKM}{4\pi^2\alpha}\sigma_L(x, Q^2), \tag{7}$$

$$F_2(x, Q^2) = \frac{K}{4\pi^2\alpha}\frac{\nu}{(1 + \nu^2/Q^2)}[\sigma_T(x, Q^2) + \sigma_L(x, Q^2)], \tag{8}$$

In order to extract the F_1, F_L and F_2 structure functions from cross section measurements the separation of the longitudinal and transverse contributions to the total cross section is required. This L/T separation is typically done experimentally by employing the Rosenbluth technique [1] which involves acquiring measurements at (at least) two but preferably more ϵ values at fixed x and Q^2 and then performing a linear fit to the reduced cross section, $\frac{d^2\sigma}{d\Omega dE'}\frac{1}{\Gamma}$, to extract σ_T and σ_L.

An example of this type of extraction is shown in Figure 1 where the inclusive reduced cross section measured on a deuterium target is plotted at fixed x and Q^2 as a function of ϵ. Each point corresponds to a different setting of beam energy, scattered electron energy and angle. The linear fit shown by the dashed line provides σ_L as the slope and σ_T as the intercept. The fit results are sensitive to the point-to-point uncertainty of the reduced cross section, the number of ϵ points utilized as well as the overall ϵ range used for fitting. To increase the accuracy of the extraction a very good control of the point-to-point uncertainties is required as well as a wide and detailed coverage in ϵ. This is a specialized type of measurement where a variety of experimental configuration changes (beam energies, scattering angles, scattered lepton energies) are required in a short time interval. It is, however, a crucial measurement to perform as it yields the fundamental quantity of R which relates the experimental observables - the cross sections - to the objects of the theoretical model - the structure functions.

To illustrate, in Figure 2 top, left panel we show cross sections measured on a hydrogen target at Jefferson Lab during the 6 GeV program in the Deep Inelastic Scattering region at relatively low $Q^2 < 2.5$ GeV^2 and x between 0.1 and 0.5. To calculate the F_2 structure function from cross sections the quantity R is needed and in this case we employ the widely used parametrization of R from SLAC, R1990 [9], and display the structure function results in

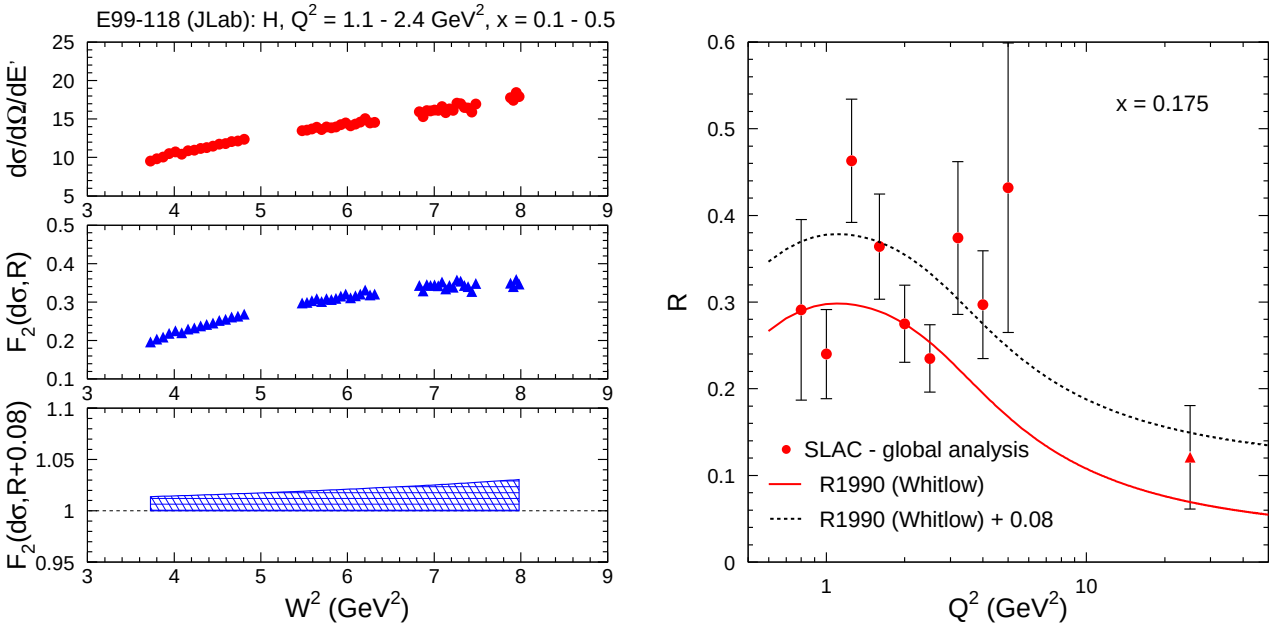

FIG. 2: **Left:** Cross section measurements from E99-118 (JLab) [36] in the deep inelastic region. R from R1990 is used to extract the F_2 structure function from cross sections. The bottom panel shows the sensitivity of the F_2 structure function to a 0.08 change in R. **Right:** R extracted by Whitlow *et al.* (R1990) [9] from a global analysis of SLAC experiments at x = 0.175. The red curve is the global fit to data while the dashed black curve shows a deviation of +0.08 from the global fit.

the middle, left panel. At this particular kinematics the quantity R takes values ranging between 0.2 and 0.3. To set a scale for the sensitivity of the F_2 structure function extraction to R in this kinematic regime we allow R from R1990 to vary by 0.08. The assumption that such fluctuation is possible is supported by the data used to constrain the R1990 parametrization at x of 0.175 as shown in Figure 2, right panel. A 0.08 change in R translates in a 2 to 4% variation in the F_2 structure function (Figure 2, bottom, left panel). In other words, an absolute uncertainty of 0.08 in R leads to a 2 to 4% uncertainty in the F_2 structure function. Precise determinations of structure functions requires knowledge of R with high accuracy.

Another instance where knowledge of R becomes important is the interpretation of the cross sections ratio σ_A/σ_D. The ratio σ_A/σ_D which has been extensively measured over the years to study nuclear medium modifications of the nucleon structure is connected to the structure functions ratio, $F_A^{1,2}/F_D^{1,2}$, via R, in particular via $\Delta R = R_A - R_D$. More often than not the measured cross section ratio is assumed to be identical to the structure function ratio but this is true only in the limit of $\epsilon = 1$ for F_2 or $\epsilon = 0$ for F_1 or if $R_A - R_D = 0$ as seen from the equations below:

$$\frac{\sigma_A}{\sigma_D} = \frac{F_2^A(x,Q^2)}{F_2^D(x,Q^2)}\frac{1+R_D}{1+R_A}\frac{1+\epsilon R_A}{1+\epsilon R_D} \approx \frac{F_2^A(x,Q^2)}{F_2^D(x,Q^2)}\left[1 - \frac{\Delta R(1-\epsilon)}{(1+R_D)(1+\epsilon R_D)}\right] \tag{9}$$

$$\frac{\sigma_A}{\sigma_D} = \frac{F_1^A(x,Q^2)}{F_1^D(x,Q^2)}\frac{1+\epsilon R_A}{1+\epsilon R_D} = \frac{F_1^A(x,Q^2)}{F_1^D(x,Q^2)}\left[1 + \frac{\epsilon \Delta R}{(1+\epsilon R_D)}\right]. \tag{10}$$

Thus in order to access $F_A^{1,2}/F_D^{1,2}$ from cross section measurements one must determine $R_A - R_D$. The unseparated cross section ratio of nuclear targets to deuterium can be related to the difference $R_A - R_D$ by

$$\frac{\sigma_A}{\sigma_D} = \frac{\sigma_A^T}{\sigma_D^T}\left[1 + \frac{\epsilon}{1+\epsilon R_D}(R_A - R_D)\right]. \tag{11}$$

The quantity $R_A - R_D$ can be extracted via the Rosenbluth technique by performing a linear fit of the A/D cross section ratios at fixed x and Q^2 at different $\epsilon^{/}$ settings. An example of such extraction from the SLAC experiment E140 [2] is shown in Figure 3 where the cross section ratios of gold and iron to deuterium targets are fitted to extract

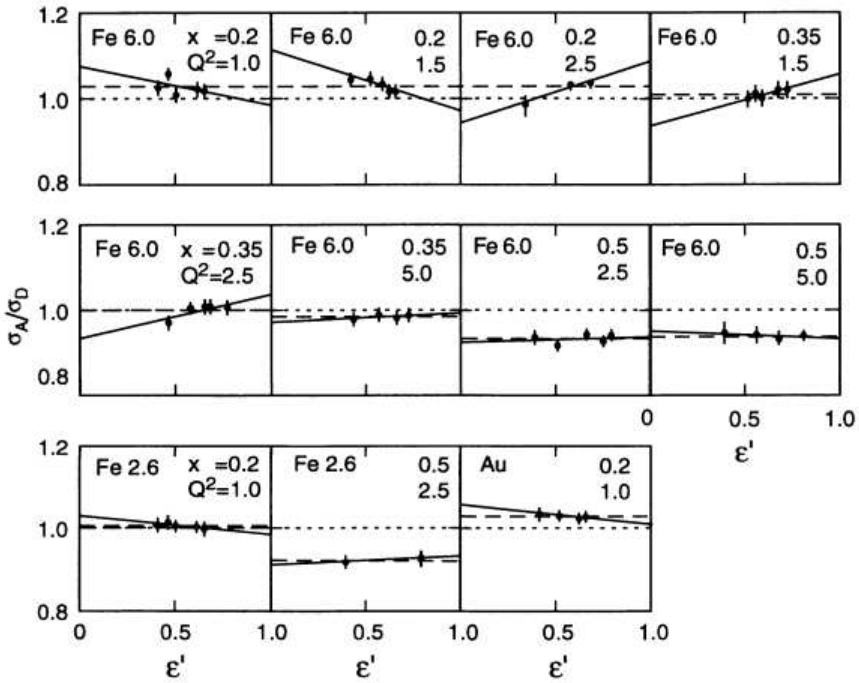

FIG. 3: An example of $R_A - R_D$ extraction on iron and gold targets from the SLAC experiment E140 [2]. Here $\epsilon^{/}$ is defined as $\frac{\epsilon}{(1+\epsilon R_D)}$. Figure taken from [2].

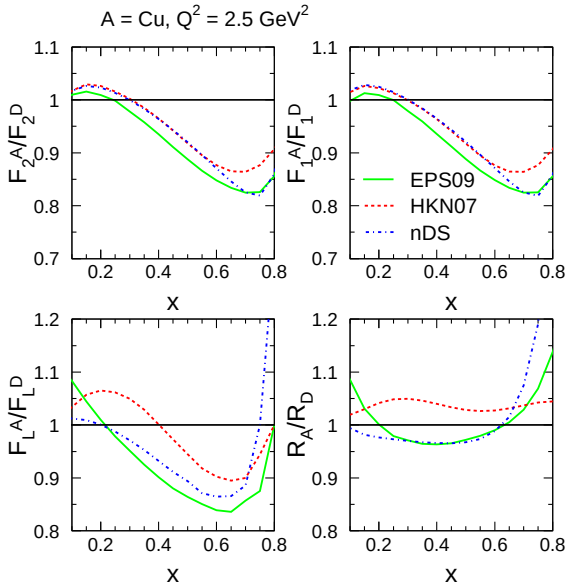

FIG. 4: An example of nuclear medium modifications of the F_2, F_1, F_L and R quantities as obtained from nuclear parton distribution functions fits from the EPS09, HKN07 and nDS collaborations [3–5].

$R_{Au} - R_D$ and $R_{Fe} - R_D$, respectively. Regarding the accuracy of this type of extraction, the same reasoning applies as for the measurement of the individual R but in addition a smaller systematic uncertainty is expected for the $R_A - R_D$ than for individual R as many of the systematics on the cross sections will cancel in the ratio.

Surprisingly there are very few *dedicated experiments* that applied the Rosenbluth technique to extract R and $R_A - R_D$ in a model-independent fashion in the DIS kinematic region ($W^2 > 4$ GeV^2). This is also reflected by the spread in nuclear parton distribution function extractions (nPDFs) from various collaborations [3–5] for quantities

like F_L and R as seen in Figure 4. For these extractions only measurements of unseparated σ_A/σ_D cross section ratios (which are very often equated to F_2^A/F_2^D ratios) are used.

II. PHYSICS MOTIVATION

A. Current Status of R Measurements on Proton and Nuclear Targets in the DIS region

In what follows we summarize existing measurements of R and $R_A - R_D$ in the DIS kinematic region at low to intermediate Q^2 making a distinction between model-independent Rosenbluth measurements and model-dependent extractions.

1. R_p and $R_d - R_p$

The only published model-independent Rosenbluth extractions of R_p and $R_d - R_p$ in DIS at low to intermediate Q^2 come from the SLAC experiment E140x [6] and the Jefferson Lab experiment E99-118 [7]. The kinematic coverage of these measurements in x and Q^2 as well as R_p and $R_d - R_p$ are shown in Figure 5. The scarcity of measurements above Q^2 of 1 GeV^2 is evident. The difference between R_d and R_p appears to be negative for $Q^2 < 1.5$ GeV^2. In [7] a global average of $R_d - R_p$ was determined which included the NMC model-dependent extraction [8] (not shown here) and it was found to be -0.054 $\pm$ 0.029. With a typical absolute value of R of 0.3 in this kinematic regime this difference amounts to a 18 $\pm$ 10% nuclear medium effect in deuterium.

Most experiments are not setup to extract R and structure functions from cross section measurements at the same time and they rely on existing parametrizations of R to transition from cross sections to structure functions. One of the most utilized fits of R in the kinematic region of $Q^2 < 20$ GeV^2 and x between 0.1 and 0.9 is the R1990 parametrization [9] obtained from a global analysis of SLAC hydrogen and deuterium data accumulated during various experiments between 1970 and 1985. Figure 6 displays the model-dependent extraction of R (data and fit) as obtained from the SLAC global analysis by Whitlow *et al.* [9]. This analysis utilized cross section measurements from eight SLAC experiments, seven of which were normalized to the cross sections from E140 [2], the only experiment that was setup to extract R on deuterium and nuclear targets via the model-independent Rosenbluth technique. The normalization factors were obtained by fitting all cross section data to a smooth model with floating parameters for each experiment and they ranged between 1 and 5% for both hydrogen and deuterium. The normalized cross sections were then binned in intervals of x and Q^2 and a bin-centering correction was applied. To extract $R(x, Q^2)$ at the center of each bin, the cross section values were linearly regressed versus ϵ. Each value of R was typically extracted from six cross section measurements from *four experiments* covering an ϵ range of about 0.5. Utilizing this procedure R_p and R_d were extracted and also $R_d - R_p$ by regressing the deuterium to hydrogen cross section ratios versus $\epsilon^{/} = \epsilon/(1 + \epsilon R_p)$. Then $R_d - R_p$ was averaged over the full kinematic range in x and Q^2 and a value of -0.001 $\pm$ 0.009 $\pm$ 0.009 was obtained. In light of this result, the extracted R_d and R_p were combined to yield the R shown in Figure 6.

This is a detailed analysis where an accurate method of mutually normalizing data sets has been employed and the propagation of systematic uncertainties that exploited all known correlations has been made but the fact still remains that given the availability of data this analysis relied on several assumptions. One assumption was that measurements from all experiments should be normalized to the results from E140, and another was that all experiments have accounted for all possible uncertainties with high accuracy. Considering that at a given x and Q^2 R is extracted from cross section data accumulated during different experiments, the validity of these assumptions directly impacts the result and precision of this R extraction. R is a fundamental quantity and the accuracy of its experimental determination directly affects our knowledge of structure functions. It is therefore critical to accumulate measurements in dedicated experiments that would allow a model-independent extraction of R via the Rosenbluth technique over a wide of kinematic range as possible.

2. $R_A - R_D$

While the nuclear dependence of the inclusive cross sections in unpolarized lepton scattering has been measured to good precision (typically a few percent) over a large kinematic region, relatively little is known of the nuclear dependence of the individual structure functions, particularly F_1 and F_L. In fact, although it is often *assumed* that the nuclear cross section ratio (σ_A/σ_D) is equivalent to the F_2 ratio, this is not a well founded assumption, especially for ϵ values far from one. As can be seen from Equations 9 and 10, the cross section ratios are only equal to the F_2

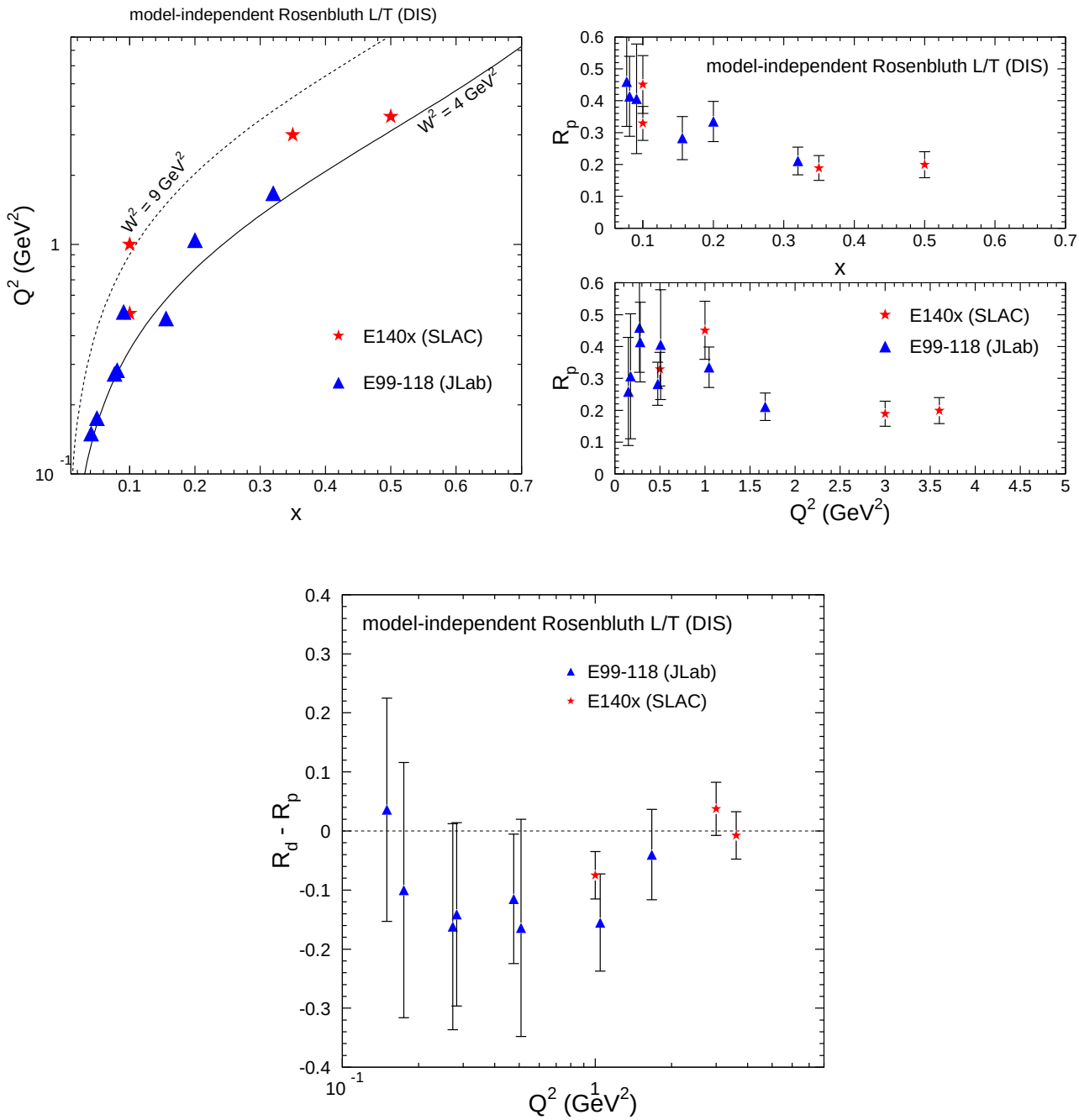

FIG. 5: **Top, left:** Kinematic coverage in x and Q^2 of model-independent Rosenbluth extractions of R_p and $R_d - R_p$ in the DIS region at small to intermediate Q^2. **Top, right:** R_p vs x and Q^2 from SLAC E140x [6] and JLab E99-118 [7]. **Bottom:** Model-independent Rosenbluth extraction of $R_d - R_p$ from E140x and E99-118.

ratios at all ϵ if $R_A = R_D$, in which case the nuclear dependence is the same for all the structure functions, F_2, F_1, and F_L. However, such an equivalence is far from being established based on the data shown in Figure 7. A determination of the nuclear dependence of the individual structure functions is necessary for a complete understanding of the origin of the EMC effect and of the cross section ratio enhancement in the antishadowing region.

At this point it is worth noting several aspects in regards to the DIS data shown in Figure 7, left panel. First, the uncertainties on most of the individual data for R_A/R_D (or $R_A - R_D$) are typically larger than 30-50% making it difficult to draw firm conclusions. Second, while the data in Figure 7 seem by eye close to unity, it is crucial to

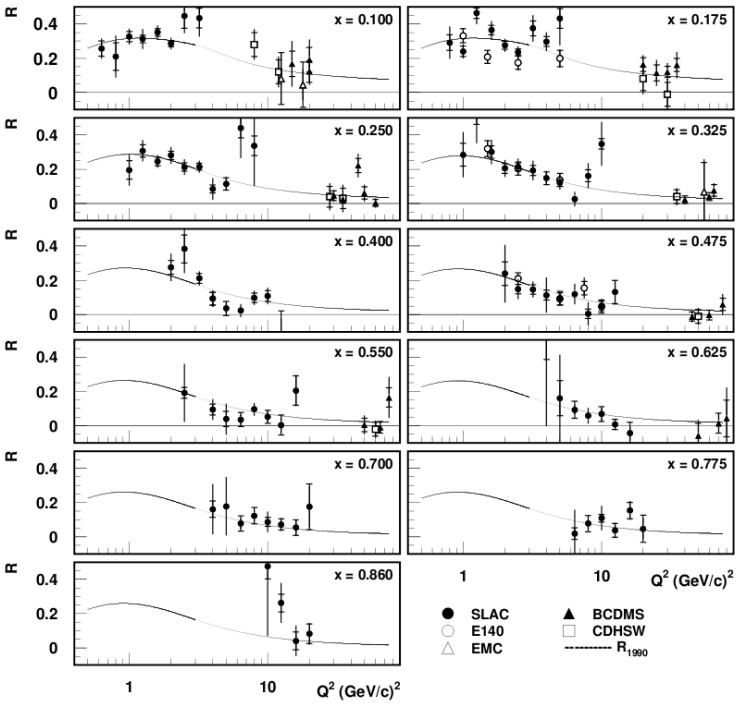

FIG. 6: Values of R from the global analysis of Whitlow *et al.* [9]. The errors shown on all SLAC data do not include the ± 0.025 systematic uncertainty due to radiative corrections. Figure taken from [9].

remember that the value of R, depending on kinematics, ranges between 0 and 0.3, and is larger at low Q^2 values where it is both easier to measure and also where a potential deviation from unity is observable. Only the SLAC experiment E140 [2] performed model-independent Rosenbluth separations on nuclear targets at few kinematic points and their results are shown in Figure 7, right panel. The HERMES [10] extractions at low x were performed with a single beam energy, providing no lever arm in ϵ at fixed x and Q^2. The NMC data [11, 12] used multiple beam energies but extracted $R_A - R_D$ using a Q^2 dependent fit at fixed x. Finally, the SLAC $R_A - R_D$ extractions, though model-independent determinations of $R_A - R_D$, were performed utilizing cross sections without Coulomb corrections applied. As it will be discussed in a later section, a recent re-extraction of $R_A - R_D$ [13] including the neglected Coulomb corrections, as well as additional data from JLab, hint that $R_A < R_D$ for Q^2 of a few GeV^2 and x in the region of the EMC effect. This case is further strengthened by the *preliminary* data from JLab experiments E04-001, E02-109, and E06-009, which focused on the extraction of $R_A - R_D$ and R_D in the **nucleon resonance region**, for $0.1 < Q^2 < 4$ GeV^2 [14]. The preliminary results for copper in the range $2 < Q^2 < 4$ GeV^2 from [14] are shown in Figure 8. These results are expected to be finalized and submitted for publication in the next month, however, the observation of nuclear dependence will remain unchanged. **The current proposal would extend the existing JLab measurements from the resonance region well into the DIS regime, W^2 up to 10 GeV^2, covering a significant range in x and Q^2 to determine whether the nuclear effects in the EMC and antishadowing regions are the same in F_1, F_2, and F_L.**

B. Implications of a Possible Nuclear Dependence of R

1. *The Antishadowing Region*

The well known behavior of modifications of the nucleus to deuteron cross section ratio σ_A/σ_D obtained from electron scattering has the pattern shown in Figure 9, left panel. For small x values, in the *shadowing region*, $x < 0.05 - 0.1$ the ratio is suppressed - the suppression increases with increasing A and a decrease of x. For $0.1 < x < 0.3$, the *antishadowing region*, the ratio is enhanced (few percent effect) with no obvious A dependence. In the interval $0.3 < x < 0.8$ the ratio is suppressed and this is called the *EMC effect*. Finally, for $x > 0.8$ the ratio increases dramatically above unity and this is attributed to nucleon motion inside the nucleus (Fermi motion). Various

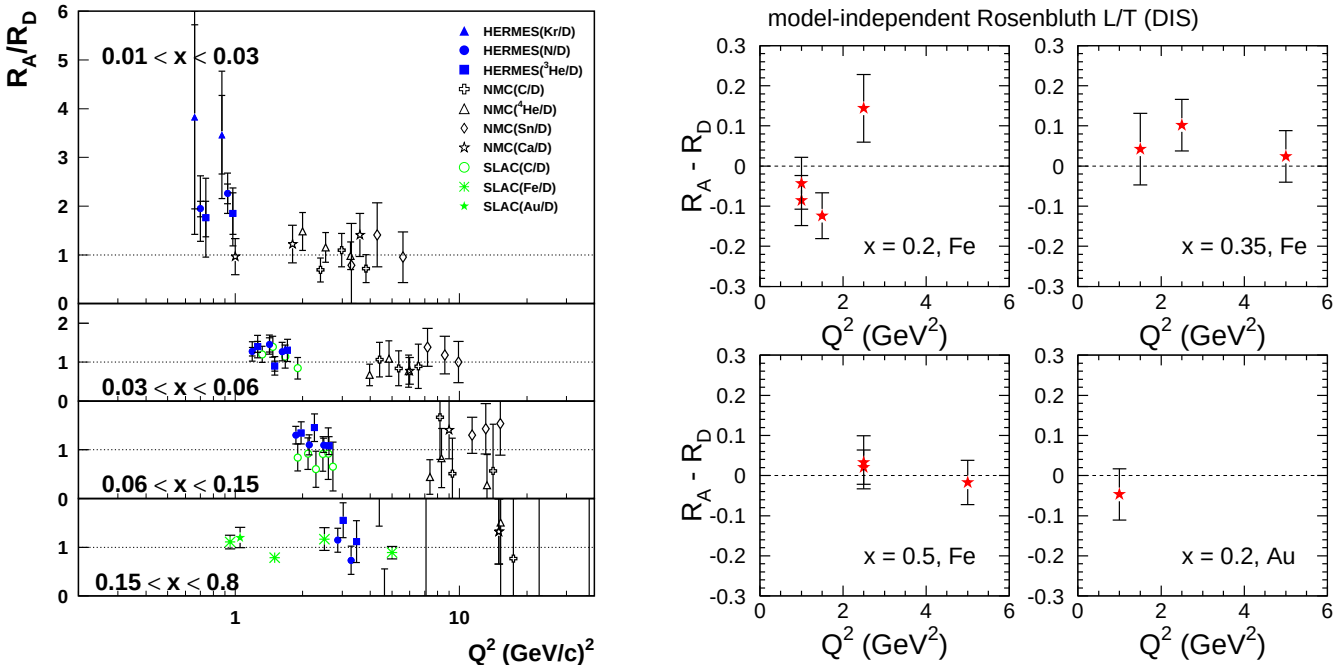

FIG. 7: **Left:** World data on R_A/R_D. Model-dependent extractions are included together with the few SLAC data from true Rosenbluth LT separations (see text). **Right:** The only published model-independent Rosenbluth extractions of $R_A - R_D$ in DIS from E140 [2].

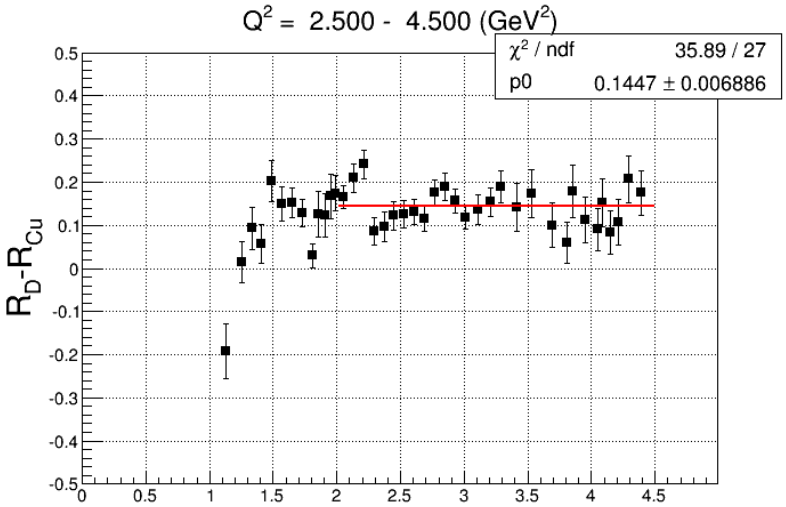

FIG. 8: Preliminary results from Hall C JLab [14] showing that $R_{Cu} < R_D$ in the resonance region. On the x-axis the quantity W^2 is shown. The typical absolute value of R_{Cu} is 0.3 thus the measured nuclear medium effect is of the order of 48%. The error bars on the data points represent the statistical and point-to-point systematic uncertainties.

models attempt to describe the nuclear modification of the experimental ratio σ_A/σ_D but there is no comprehensive understanding of the entire pattern.

Unlike the shadowing effect, antishadowing shows little or no sensitivity to A within experimental uncertainties, for example, in the SLAC E139 [15] and NMC data [12]. While antishadowing is observed in nuclear DIS, it remains something of a mystery why the cross section enhancement is not seen in nuclear Drell-Yan ratios [16] (Figure 9, right panel) nor in the total neutrino-nucleus cross sections for $x > 0.1$ [17]. The deviation of σ_A/σ_D from unity in this region is of the order of a few percent and most measurements quote normalization uncertainties on the order of 1-2%

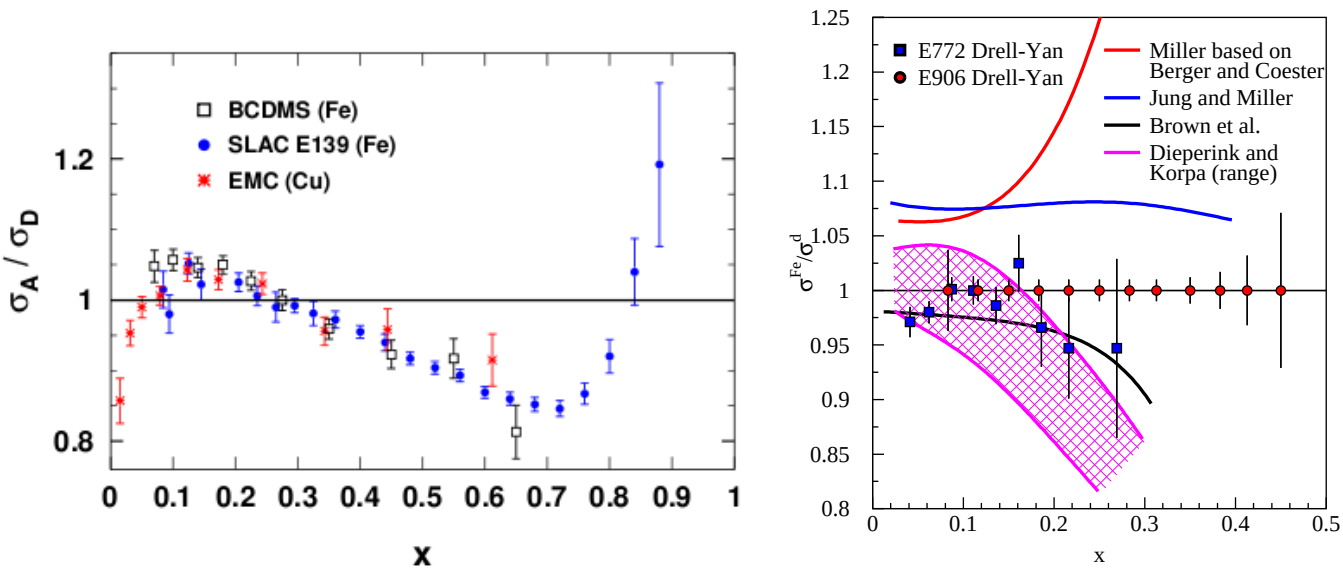

FIG. 9: **Left:** Nuclear modifications of the cross section ratio σ_A/σ_D as a function of x for iron and copper. The data are from BCDMS [18] (open squares), SLAC E139 [15] (filled circles) and EMC [19] (stars). **Right:** Cross section ratio of iron to deuterium from Drell-Yan experiments E772 [16] (filled squares) and projections from E906 [20] (filled circles) as a function of x. The ratio from E772 showed **no** enhancement in the antishadowing region, with limited precision. E906 is underway.

so it is difficult to quantify the absolute size of the antishadowing effect precisely. From the theory perspective, in the leading twist formalism, the small enhancement of the cross section ratio in the antishadowing region translates into an enhancement of the valence quark and possibly gluon distributions in nuclei in this region [3, 4]. But the pattern and especially the magnitude of nuclear modifications of the gluon distribution in nuclei are very poorly constrained by present data.

A recent study by V. Guzey *et al.* [21] examined the impact of the nuclear dependence of R on the extraction of the nucleus to deuteron structure function ratios, F_2^A/F_2^D and F_1^A/F_1^D from σ_A/σ_D data. Guzey and collaborators demonstrated that in the presence of a small but non-zero difference between R for nuclei and the nucleon, the nuclear enhancement in the ratio of the transverse structure functions F_1^A/F_1^D becomes significantly reduced (or even disappears in some cases), indicating that antishadowing may be dominated by the longitudinal contribution.

The study used a compilation of measurements of the nuclear dependence of R as shown in Figure 10. It was pointed out in their study that the nuclear dependence of R has not yet being systematically measured using the Rosenbluth technique so two assumptions for ΔR were explored: (absolute, black-dashed) $\Delta R = R_A - R_D = 0.04$ and (relative, black-dotted) $(R_A - R_D)/R_N = 30\%$. The first assumption was based on the NMC measurements of $R_{Sn} - R_C$ at an average Q^2 of 10 GeV^2 (Figure 10). The second assumption was possible in view of the fact that the NMC Sn/C data allows for a 22 to 120% relative deviation of $\Delta R/R_N$ because of the large uncertainties. It was effectively assumed that $R_A - R_D = R_{Sn} - R_C$ which corresponds to a lower limit for ΔR.

Taken from their study, the impact of these assumptions on selected nuclear DIS data is presented in Figure 11. The low x and high x data points have been neglected the focus being on the antishadowing region. The BCDMS Fe/D, EMC Cu/D and NMC Ca/D data shown in Figure 11, left panel, correspond to ϵ close to unity. So regardless of the assumption for ΔR, one expects that $F_2^A/F_2^D \approx \sigma_A/\sigma_D$ with a very good accuracy. On the other hand, F_1^A/F_1^D is clearly smaller than σ_A/σ_D. Thus, the few percent enhancement of the cross section ratio in the antishadowing region may be reduced or removed altogether for the ratio of the transverse structure functions F_1^A/F_1^D if there is in fact a nuclear dependence of R.

For the SLAC E139 and E140 Fe/D data presented in Figure 11, right panel, the values of Q^2 are rather small and the assumptions for the nuclear dependence of R motivated by the NMC Sn/C measurement at higher Q^2 require a significant extrapolation in Q^2. Since the values of ϵ for these two data sets are not close to unity $\Delta R > 0$ leads to noticeable differences between the ratio of the structure functions and the ratio of the cross sections according to the trend described by Equations 9, 10: $F_1^A/F_1^D < \sigma_A/\sigma_D < F_2^A/F_2^D$. Thus the assumed nontrivial nuclear dependence of R leads to a decrease or to a complete disappearance (in some case) of enhancement of the F_1^A/F_1^D structure function ratio in the $0.1 < x < 0.3$ region.

This recently published study highlighted the lack of precision measurements of $R_A - R_D$ and showed that even

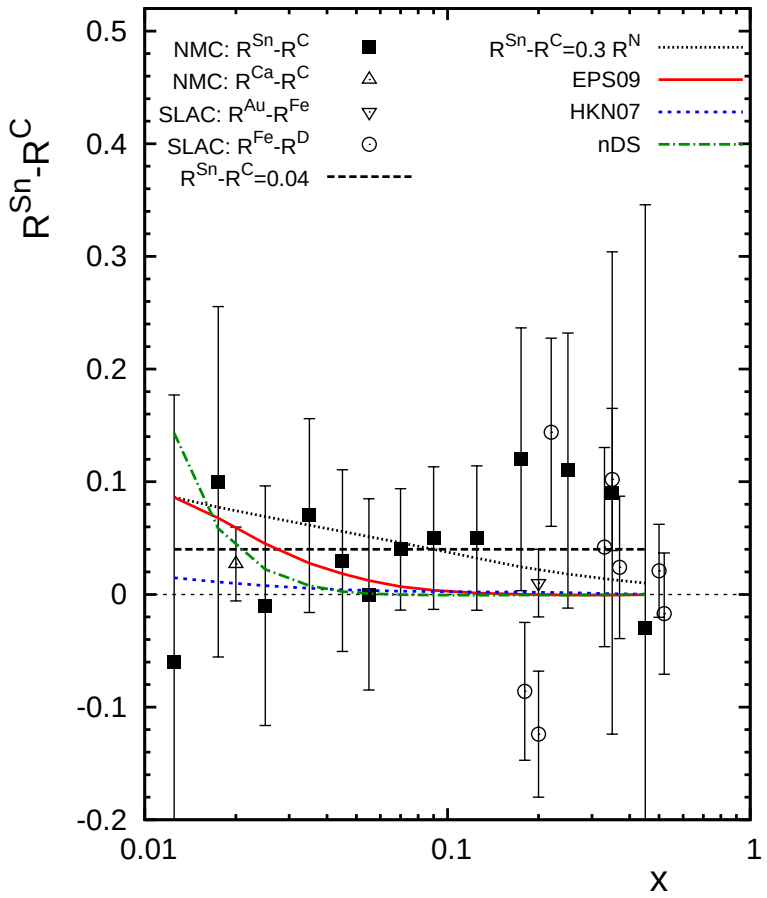

FIG. 10: $R_{Sn} - R_C$ as a function of x. Full squares are results of the NMC measurement with statistical and systematic errors added in quadrature [11]; the long-dash and dotted curves correspond to $R_{Sn} - R_C = 0.04$ and $R_{Sn} - R_C = 0.3R_N$, respectively; the curves labeled $EPS09$, $HKN07$ and nDS correspond to predictions using different nuclear parton distributions. Also shown are the NMC result for $R_{Ca} - R_C$ [12] (triangle), the SLAC result for $R_{Au} - R_{Fe}$ [22] (inverse triangle), and SLAC E140 results for $R_{Fe} - R_D$ as a function of x [2] (open circles). Figure taken from [21].

a small difference in $R_A - R_D$ within the large uncertainties of the available data could have a big impact on the interpretation of the cross section ratio enhancement in the antishadowing region. If a nuclear dependence is confirmed by precision experiments, this observation would indicate that the effect of antishadowing in the cross section ratio is predominantly due to the contribution of the longitudinal structure function F_L, instead of F_1 as implicitly assumed in most phenomenological analyses and global nuclear parton distribution fits.

2. *The EMC Effect Region*

At $x > 0.3$, one is exploring the canonical "EMC Effect" region where there is an apparent and well-explored suppression of the inclusive electron scattering cross section from a nucleus. As noted earlier, in most measurements of the EMC effect, it has been assumed that the cross section ratio is immediately identifiable with the ratio of structure functions, i.e., $\sigma_A/\sigma_D = F_2^A/F_2^D$. This identification of course presumes no (or small) nuclear dependence of R for values of $\epsilon < 1.0$.

The assumption that $R_A = R_D$ at large x has been investigated (see Fig. 7) and no evidence for a *significant* nuclear dependence of R has been seen in published measurements to date. However, a couple of comments are in order. First, the bulk of the data shown in the bottom panel of Fig. 7 is for $x \leq 0.35$. Second, as noted earlier, only the SLAC E140 experiment performed a true Rosenbluth separation. Other measurements (HERMES and NMC) performed fits at multiple values of ϵ, but not necessarily at fixed Q^2, so assumptions had to be made regarding the Q^2 dependence of both the structure function ratios and the nuclear dependence of R. The most precise measurements relevant to

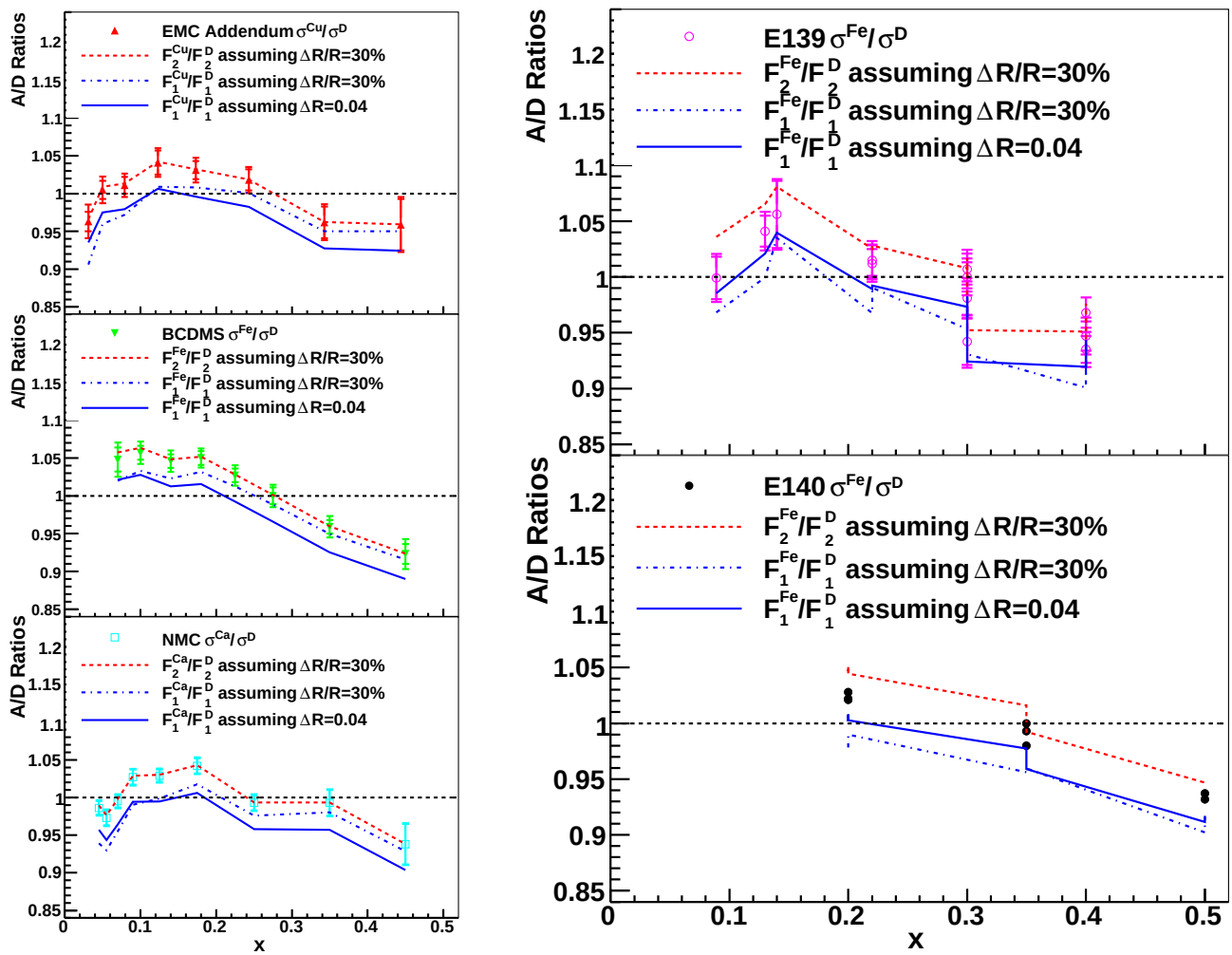

FIG. 11: **Left:** The impact of the nontrivial nuclear dependence of R on the structure function ratios around the antishadowing region for BCDMS Fe/D [18], EMC Cu/D [19] and NMC Ca/D [12] data. The values of ϵ are close to unity. **Right:** Similar study on SLAC E139 [15] and E140 [2] iron to deuterium data. Figures taken from [21].

the "EMC region" come from SLAC E140, at $x = 0.5$. Moreover, as we have seen in the previous subsection, it does not take a *significant* nuclear medium modification of R to change how we interpret the structure functions ratio $F^A_{1,2}/F^D_{1,2}$.

Recently, the SLAC E140 results have been re-analyzed including the effects of the acceleration (deceleration) of the incident (scattered) electron in the Coulomb field from the extra protons of the nuclear target [13]. The ϵ dependence of the σ_A/σ_D ratios is shown in Fig. 12 for the re-analyzed SLAC E140 data (iron target) at $x = 0.5$ and $Q^2 = 5$ GeV^2. In addition, data from SLAC E139 and preliminary copper data from JLab E03103 have been included in the fit. Where the original E140 results yielded a value of $R_A - R_D$ consistent with zero ($-0.017 \pm\ 0.054$) on average, the updated combined fit yields a result of $R_A - R_D = -0.084 \pm 0.045$, clearly implying a non-trivial nuclear dependence of R at large x. It is worth noting that both the sign and the magnitude of $R_A - R_D$ from this analysis are consistent with the preliminary results shown in Figure 8.

The potential consequences of the above result are difficult to overstate. The presumption for the last 30 years has been that the nuclear dependence of the cross section ratios measured in inclusive lepton scattering experiments correspond directly to modifications of the quark distribution functions. In the case of a non–zero $R_A - R_D$ the situation is significantly more complicated. As seen in Fig.12, the fit-intercept, which corresponds to F^A_1/F^D_1 is nearly 1.0 at $x = 0.5$. If F_1 displays little or no nuclear dependence at this large value of x, the implication is that the observed cross section modification comes almost entirely from the longitudinal contribution to the cross section

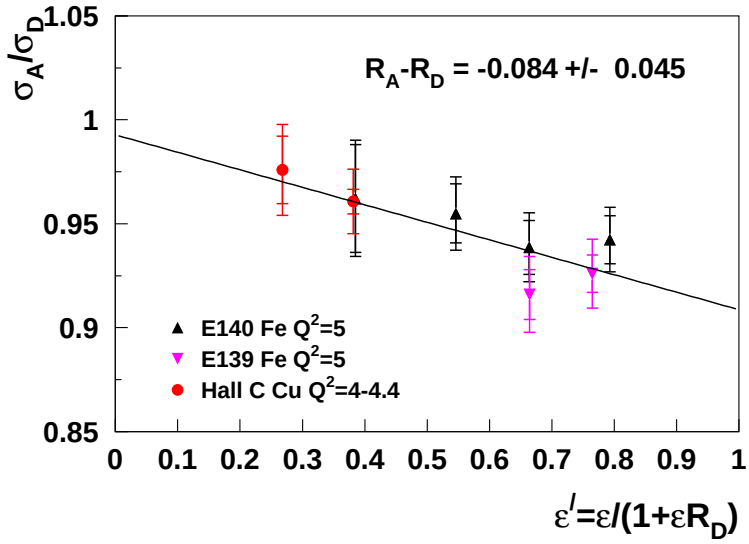

FIG. 12: σ_A/σ_D vs. $\epsilon' = \epsilon/(1+\epsilon R_D)$ at $x = 0.5$, $Q^2 = 4-5$ GeV^2 for iron and copper ratios from SLAC E140 [2], E139 [15], and JLab E03103. The slope of the fitted line directly corresponds to $R_A - R_D$, while the intercept yields $\sigma_T^A/\sigma_T^D = F_1^A/F_1^D$.

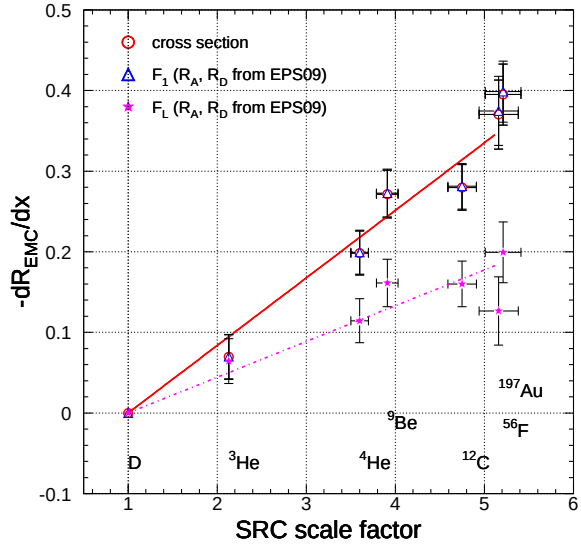

FIG. 13: Size of the EMC Effect, defined as the slope of the ratio, $-dR/dx$, between $x = 0.3$ and $x = 0.7$ vs. the SRC scale factor, $a_2 = \sigma_A/\sigma_D$ for $x > 1.4$. Red open circles show the slopes extracted from the usual EMC ratios (ratio of cross sections), while the blue triangles and magenta stars show the ratios of F_1 and F_L extracted from the cross section ratios using values of R_A and R_D from [3].

(since $F_1^A/F_1^D = \sigma_T^A/\sigma_T^D$.) Such a conclusion opens the door to very different models of the origin of the EMC effect, including contributions from spin-0 constituents. It is naturally premature to draw such significant conclusions from this re–analysis, however it is clear that the questions raised are significant enough that a larger, more precise data set is urgently needed.

Recently, significant insight into possible origins of the EMC effect has been obtained through comparisons of the slope of the EMC ratio dR/dx between $0.3 < x < 0.7$ compared to the ratio $a_2 = \sigma_A/\sigma_D$ in the region $x > 1$ [23–25].

The ratio a_2 is sensitive to the relative number of short-range correlations (SRCs) in a nucleus, another quantity of much interest in its own right. The comparison of the size of the EMC effect to the number of short range correlations in a nucleus is illustrated in Fig. 13 where the EMC slope is plotted vs. the SRC scale factor (a_2). A significant conclusion from studies comparing the two effects is that the EMC effect and Short Range Correlations either stem from some common (as yet unknown) origin or that the SRC ratio serves an effective measurement of some quantity like nucleon virtuality or local density experienced by a nucleon participating in a correlated pair, which in turn gives rise to the EMC effect. These conclusions are drawn from the fact that the correlation between the two observables is quite robust, and that both even measure the same relative effect for a nucleus like beryllium, which has a relatively small average density, but whose EMC effect is more comparable to a nucleus with a higher average density like carbon [26].

However, once one considers the possibility that R is an A-dependent quantity, the interpretation becomes more complicated. If the EMC effect and SRCs exhibit such an excellent correlation, but the size of the EMC effect is in part coming from contributions from longitudinal photons, what does this imply about the underlying cause of either, or both? Is the view that both stem from a common origin still tenable?

In addition to the more commonly plotted target ratios, Fig. 13 also shows the EMC effect slope one would extract for the F_1 and F_L structure functions, using the EPS09 fit for R_A and R_D [3]. Even when constrained by the existing world data (which one should recall is rather sparse at large x), one can see a significant difference between the size of the ratio slopes between the two structure functions. Yet, interestingly, the correlation between the EMC slope and the SRC scale factor is quite good for either quantity.

As shown above, studies of the EMC effect have achieved sufficient quantitative precision that the current experimental situation regarding the nuclear dependence of R is wholly unacceptable. While earlier measurements had suggested that $R_A - R_D$ was small or zero, the more recent re-analysis suggests this may not be the case. The recently observed connection between the EMC effect and Short Range Correlations is very exciting, but the interpretation must remain somewhat ambiguous until it is established whether this connection applies in the same way to all components (F_1, F_2, F_L) of the inclusive cross section.

III. PROPOSED MEASUREMENTS

We propose to measure with unprecedented statistical precision inclusive inelastic electron-nucleon and electron-nucleus scattering cross sections in the DIS regime (x from 0.1 to 0.6 and Q^2 from 1 to 5 GeV^2) on hydrogen, deuterium, carbon, copper and gold targets to extract R_p, $R_d - R_p$, R_A, $R_A - R_D$, F_L, F_1 and F_2 in an model independent fashion. We choose copper as a heavy enough nucleus for observations of nuclear medium modifications of R and of the separated structure functions to map the kinematic dependence of this effects in both x and Q^2. In conjunction with copper, carbon and gold will then map the A dependence of the effect. Carbon has also the advantage of being a isoscaler nucleus thus no isoscaler corrections will be necessary and also is a light enough nucleus that the Coulomb corrections are expected to be small. Measurements on hydrogen and deuterium targets will provide a comprehensive study of $R_d - R_p$ in the DIS regime and also much needed model-independent extractions of R_p and of the separated proton structure functions.

We will use the well suited standard Hall C 12 GeV equipment, the High Momentum Spectrometer (HMS) and the Super-High Momentum Spectrometer (SHMS). We need 4 cm cryogenic hydrogen and deuterium targets as well as 2% radiation length (r.l.) solid targets carbon, copper, and gold. An aluminum target will only be used to measure background coming from the walls of the hydrogen and deuterium targets. To achieve the best possible precision for our measurements of σ_L and σ_T, 6 beam energies are required: 4.4, 5.5, 6.6, 7.7, 8.8 and 11 GeV (two of these are non-standard beam energies). Given the superior figure of merit of JLab the improvement in the statistical precision will be up to a factor of 4 when compared to SLAC E140 [2].

In what follows we detail the choice of kinematics, we present the physics rates calculations and estimates of expected backgrounds and corrections to the proposed cross sections. We outline the beam-time estimates needed to achieve the desired statistical precision and we discuss the impact of our proposed measurements.

Summary of changes with respect to the previous proposal submission

We submitted a previous version of this proposal to PAC40. We received very good suggestions and we were encouraged to resubmit our proposal. In particular we were asked to reduce the broad scope of our initially proposed physics program by making a selection of few targets (light and heavy) from beryllium, carbon, copper, silver and gold to carry an initial search of medium modifications of R. Below we outline the modifications we made to our proposal following the suggestions made by PAC40.

- We eliminated beryllium and silver as targets; we believe that carbon, copper and gold will be sufficient for a mapping of medium modifications of R and of the separated structure functions F_1, F_L and F_2.

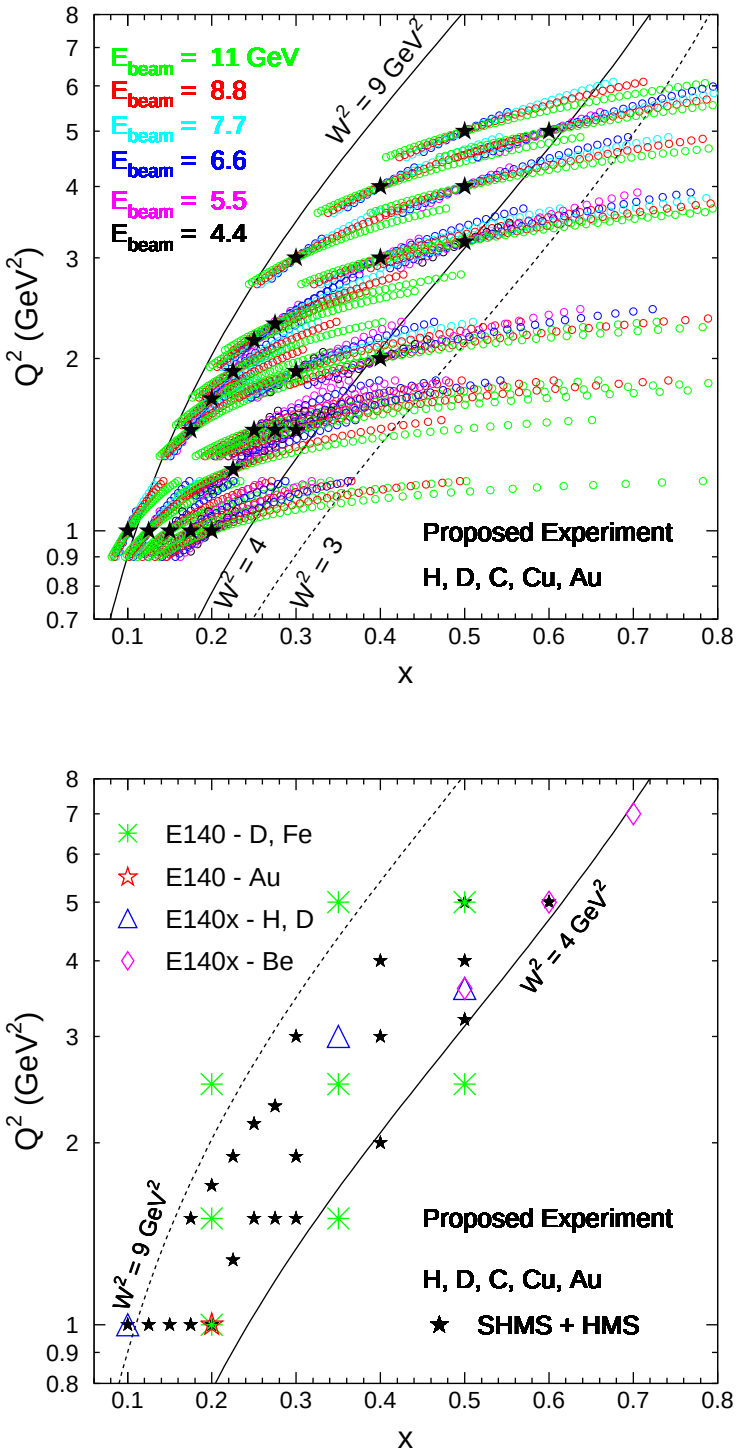

FIG. 14: **Top:** Proposed central kinematics shown in black stars together with the coverage given by the momentum acceptance of the Hall C spectrometers HMS and SHMS indicated by empty circles on a Q^2 vs x grid. The angular acceptance of the spectrometers is not shown here as we plan to extract the cross sections at fixed central angle by averaging over the angular acceptance after kinematic corrections. The solid and dotted curves indicate the W^2 coverage our focus being roughly on the region of W^2 from 3 to 10 GeV^2. **Bottom:** Our proposed central kinematic coverage compared to that of the SLAC experiments E140 [2] and E140x [6]. The statistical uncertainty for the SLAC experiments varies between 0.6% and 2.2% while we aim to achieve a statistical precision of 0.2% to 0.5% along with an expanded kinematic sensitivity to study any x and/or Q^2 dependence separately.

x	Q^2	E_B	E_p	θ	ϵ
0.100	1	6.6	1.271	19.881	0.356
0.100	1	7.7	2.371	13.440	0.551
0.100	1	8.8	3.471	10.381	0.673
0.100	1	11	5.671	7.259	0.809
0.125	1	5.5	1.237	22.104	0.406
0.125	1	6.6	2.337	14.629	0.613
0.125	1	7.7	3.437	11.155	0.732
0.125	1	8.8	4.537	9.077	0.805
0.125	1	11	6.736	6.659	0.885
0.150	1	4.4	0.847	30.015	0.338
0.150	1	6.6	3.047	12.802	0.745
0.150	1	8.8	5.247	8.439	0.871
0.150	1	11	7.447	6.333	0.923
0.175	1	4.4	1.355	23.633	0.526
0.175	1	5.5	2.455	15.641	0.721
0.175	1	6.6	3.555	11.849	0.819
0.175	1	8.8	5.755	8.058	0.907
0.175	1	11	7.955	6.128	0.944
0.175	1.5	5.5	0.932	31.379	0.298
0.175	1.5	6.6	2.032	19.250	0.538
0.175	1.5	7.7	3.132	14.326	0.679
0.175	1.5	8.8	4.232	11.518	0.767
0.175	1.5	11	6.432	8.349	0.863
0.200	1	4.4	1.735	20.849	0.646
0.200	1	5.5	2.835	14.548	0.791
0.200	1	6.6	3.935	11.260	0.864
0.200	1	8.8	6.135	7.803	0.930
0.200	1	11	8.335	5.986	0.957
0.200	1.7	5.5	0.970	32.782	0.307
0.200	1.7	6.6	2.070	20.315	0.544
0.200	1.7	7.7	3.170	15.164	0.683
0.200	1.7	8.8	4.270	12.209	0.770
0.200	1.7	11	6.470	8.864	0.864

TABLE I: Central kinematics to measure the nuclear dependence of the ratio $R = \sigma_L/\sigma_T$ and of the separated structure functions. The units for four-momentum transferred squared Q^2, beam energy E_B, scattered electron energy E_p, and angle θ are GeV^2, GeV, GeV/c and degrees, respectively. For each fixed (x,Q^2) L/T extraction both SHMS and HMS will be used in a complementary fashion when necessary. For the deuterium and copper targets measurements will be performed at all kinematics shown while for carbon, gold and hydrogen, data will be taken only at select kinematics (see Table IV).

x	Q^2	E_B	E_p	θ	ϵ
0.225	1.28	4.4	1.368	26.657	0.521
0.225	1.28	5.5	2.468	17.663	0.717
0.225	1.28	6.6	3.568	13.388	0.816
0.225	1.28	8.8	5.768	9.108	0.906
0.225	1.28	11	7.968	6.928	0.943
0.225	1.9	5.5	1.000	34.180	0.312
0.225	1.9	6.6	2.100	21.337	0.547
0.225	1.9	7.7	3.200	15.962	0.686
0.225	1.9	8.8	4.300	12.866	0.771
0.225	1.9	11	6.500	9.350	0.865
0.250	1.5	4.4	1.203	30.877	0.456
0.250	1.5	5.5	2.303	19.817	0.677
0.250	1.5	6.6	3.403	14.849	0.790
0.250	1.5	8.8	5.603	10.006	0.893
0.250	1.5	11	7.803	7.580	0.936
0.250	2.15	5.5	0.917	38.105	0.280
0.250	2.15	6.6	2.017	23.183	0.525
0.250	2.15	7.7	3.117	17.213	0.670
0.250	2.15	8.8	4.217	13.824	0.759
0.250	2.15	11	6.417	10.012	0.858
0.275	1.5	4.4	1.493	27.643	0.555
0.275	1.5	5.5	2.593	18.663	0.736
0.275	1.5	6.6	3.693	14.250	0.828
0.275	1.5	8.8	5.893	9.756	0.912
0.275	1.5	11	8.093	7.442	0.947
0.275	2.3	5.5	1.043	36.913	0.318
0.275	2.3	6.6	2.143	23.264	0.550
0.275	2.3	7.7	3.243	17.456	0.688
0.275	2.3	8.8	4.343	14.091	0.772
0.275	2.3	11	6.543	10.256	0.866
0.300	1.5	4.4	1.735	25.606	0.628
0.300	1.5	5.5	2.835	17.841	0.780
0.300	1.5	6.6	3.935	13.802	0.856
0.300	1.5	8.8	6.135	9.561	0.926
0.300	1.5	11	8.335	7.333	0.955
0.300	1.9	4.4	1.025	37.874	0.378
0.300	1.9	5.5	2.125	23.261	0.628
0.300	1.9	6.6	3.225	17.183	0.758
0.300	1.9	7.7	4.325	13.718	0.832
0.300	1.9	8.8	5.425	11.449	0.877
0.300	1.9	11	7.625	8.632	0.926

TABLE II: Continuation of Table I. For the deuterium and copper targets measurements will be performed at all kinematics shown while for carbon, gold and hydrogen, data will be taken only at select kinematics (see Table IV).

x	Q^2	E_B	E_p	θ	ϵ
0.300	3	6.6	1.271	34.795	0.327
0.300	3	7.7	2.371	23.388	0.527
0.300	3	8.8	3.471	18.030	0.655
0.300	3	11	5.671	12.590	0.797
0.400	2	4.4	1.735	29.652	0.610
0.400	2	5.5	2.835	20.629	0.768
0.400	2	6.6	3.935	15.950	0.848
0.400	2	8.8	6.135	11.044	0.921
0.400	2	11	8.335	8.470	0.952
0.400	3	5.5	1.503	35.057	0.442
0.400	3	6.6	2.603	24.119	0.634
0.400	3	7.7	3.703	18.667	0.745
0.400	3	8.8	4.803	15.309	0.814
0.400	3	11	7.003	11.325	0.889
0.400	4	6.6	1.271	40.395	0.313
0.400	4	7.7	2.371	27.069	0.516
0.400	4	8.8	3.471	20.848	0.646
0.400	4	11	5.671	14.547	0.791
0.500	3.2	4.4	0.989	50.765	0.324
0.500	3.2	5.5	2.089	30.596	0.590
0.500	3.2	6.6	3.189	22.483	0.732
0.500	3.2	7.7	4.289	17.907	0.813
0.500	3.2	8.8	5.389	14.925	0.863
0.500	3.2	11	7.589	11.235	0.918
0.500	4	5.5	1.237	45.089	0.343
0.500	4	6.6	2.337	29.503	0.565
0.500	4	7.7	3.437	22.418	0.696
0.500	4	8.8	4.537	18.212	0.778
0.500	4	11	6.737	13.342	0.868
0.500	5	6.6	1.271	45.413	0.299
0.500	5	7.7	2.371	30.337	0.504
0.500	5	8.8	3.471	23.342	0.637
0.500	5	11	5.671	16.276	0.785
0.600	5	5.5	1.059	55.189	0.270
0.600	5	6.6	2.159	34.455	0.512
0.600	5	7.7	3.259	25.791	0.658
0.600	5	8.8	4.359	20.799	0.750
0.600	5	11	6.559	15.127	0.851

TABLE III: Continuation of Table II. For the deuterium and copper targets measurements will be performed at all kinematics shown while for carbon, gold and hydrogen, data will be taken only at select kinematics (see Table IV).

- We eliminated few Q^2 points at several values of x as follows: at x = 0.15 from Q^2 of 1 and 1.28 GeV^2 we kept 1; at x = 0.2 from Q^2 of 1, 1.28 and 1.7 we kept 1 and 1.7 GeV^2; at x = 0.275 from Q^2 of 1.5, 2.3 and 2.6 we kept 1.5 and 2.3 GeV^2; at x = 0.3 from Q^2 of 1.5, 1.9, 2.55 and 3 we kept 1.5, 1.9 and 3 GeV^2. The Q^2 points we eliminated would not have extended significantly the kinematic Q^2 coverage of our proposed measurements.

- We plan to use copper to exhaustively map the kinematic x and Q^2 dependence of nuclear medium modifications of R and of the separated structure functions F_1, F_L and F_2. Thus we will measure on copper at all kinematics shown in Tables I, II and III. Carbon and gold will be used to determine the A dependence of nuclear medium modifications thus data on these targets will be taken at select kinematics as follows: x = 0.1, x = 0.15, x = 0.2 and $Q^2 = 1.7$, x = 0.25 and $Q^2 = 1.5$, x = 0.3 and $Q^2 = 1.9$ and x = 0.4 and $Q^2 = 3$. On carbon we will also measure at x = 0.6 and $Q^2 = 5$ GeV^2.

A. Kinematics

Our goal is to perform precise L/T separations in the kinematic range of $x = 0.1$ to 0.6 covering the antishadowing and the EMC effect regions. Figure 14 shows our choice of kinematics. The black stars indicate the fixed (x , Q^2) settings each leading to one extraction at central kinematics of R_p, $R_d - R_p$, R_A, $R_A - R_D$, F_1, F_L and F_2. For each fixed (x , Q^2) setting we plan at least four and up to six ϵ points measurements each obtained by using different beam energies and central spectrometers settings in E_p and θ. Details of the kinematic coverage are also shown in Tables I, II and III. For copper and deuterium targets measurements will be performed at all kinematics shown while for hydrogen, carbon and gold only at select settings as outlined in Table IV.

Given the large momentum acceptance of the SHMS (-10% to +22%) and HMS (±8%) additional L/T extractions can be performed using the data collected within the acceptance by applying only small Q^2 corrections thus exploiting to the fullest the unique capabilities of the Hall C spectrometers. For a given central kinematic setting defined by $(x, Q^2, E_B, E_p, \theta)$ we bin the momentum acceptance of the spectrometers in intervals corresponding to a size in W^2 of 0.1 GeV^2 (each such bin is shown as an empty circle in Figure 14). At certain (x, Q^2), the fully desired ϵ-range can only be achieved using both the HMS and the SHMS. We plan to and assume that we can cross-calibrate the two spectrometers to the level of 1% precision. Some of the momentum scans that can be covered with both spectrometers will be measured with both for cross-calibration.

In Figure 14, bottom panel, we show the central kinematic coverage of our proposed measurements (black stars) compared to that of the SLAC experiments E140 [2] (stars and snowflakes) and E140x [6] (triangles and diamonds). Experiment E140 measured inclusive cross sections from electron scattering on deuterium, iron and gold targets for Rosenbluth L/T separations and extracted $R_{Fe} - R_D$ at $x = 0.2$, 0.35, 0.5 and $R_{Au} - R_D$ at x = 0.2. The number of ϵ points used per extraction varied between two to five with a statistical uncertainty at the cross section level between 0.6% and 1.3% for deuterium, 0.6% to 2.2% for iron and 0.6% to 1.4% for gold. The systematic uncertainty varied between 0.5% and 0.7%. Experiment E140x performed L/T separations on hydrogen and deuterium targets at $x =$ 0.1, 0.35 and 0.5 and on beryllium at $x = 0.5$, 0.6 and 0.7. It extracted $R_{deuterium} - R_{hydrogen}$ at x of 0.1, 0.35 and 0.5 and $R_{beryllium} - R_{hydrogen}$ at $x = 0.5$. The statistical uncertainty on this measurement was around 1% with a systematic of at most 0.8%. With our proposed measurements we plan to drastically reduce the statistical uncertainty aiming for 0.2% to 0.5% and expand the kinematic sensitivity to study any x and/or Q^2 dependence separately.

B. Physics Rates

We calculated the electron rates for the hydrogen target using the cross section model developed by M.E. Christy [27]. This is an empirical fit to measurements of inclusive inelastic electron-proton cross sections in the kinematic range of four-momentum transfer $0 < Q^2 < 8$ GeV^2 and final state invariant mass $1.1 < W < 3.1$ GeV. The fit is constrained by the high precision longitudinal and transverse separated cross section measurements from Jefferson Lab Hall C, un-separated Hall C measurements up to Q^2 of 7.5 GeV^2, and photoproduction data at $Q^2 = 0$. Compared to previous fits, this fit covers a wider kinematic range, fits both transverse and longitudinal cross sections, and features smooth transitions to the photoproduction data at $Q^2 = 0$ and DIS data at high Q^2 and W.

The electron rates on nuclear targets were calculated using the cross section model of P.E. Bosted and V. Mamyan [28]. This is an empirical fit to electron-nucleus scattering for $A > 2$ based on world data. It is valid for $0 < W < 3.2$ GeV and $0.2 < Q^2 < 5$ GeV^2. The fit is based on previous empirical fits to electron-proton and electron-neutron scattering, but takes into account the effects of Fermi motion, meson exchange currents and Coulomb corrections. A comparison of this model to JLab inclusive electron-nucleus cross section data on iron, aluminum, hydrogen, deuterium, beryllium, carbon and gold [14, 29] is shown in Figure 15 in a Q^2 range that matches the coverage

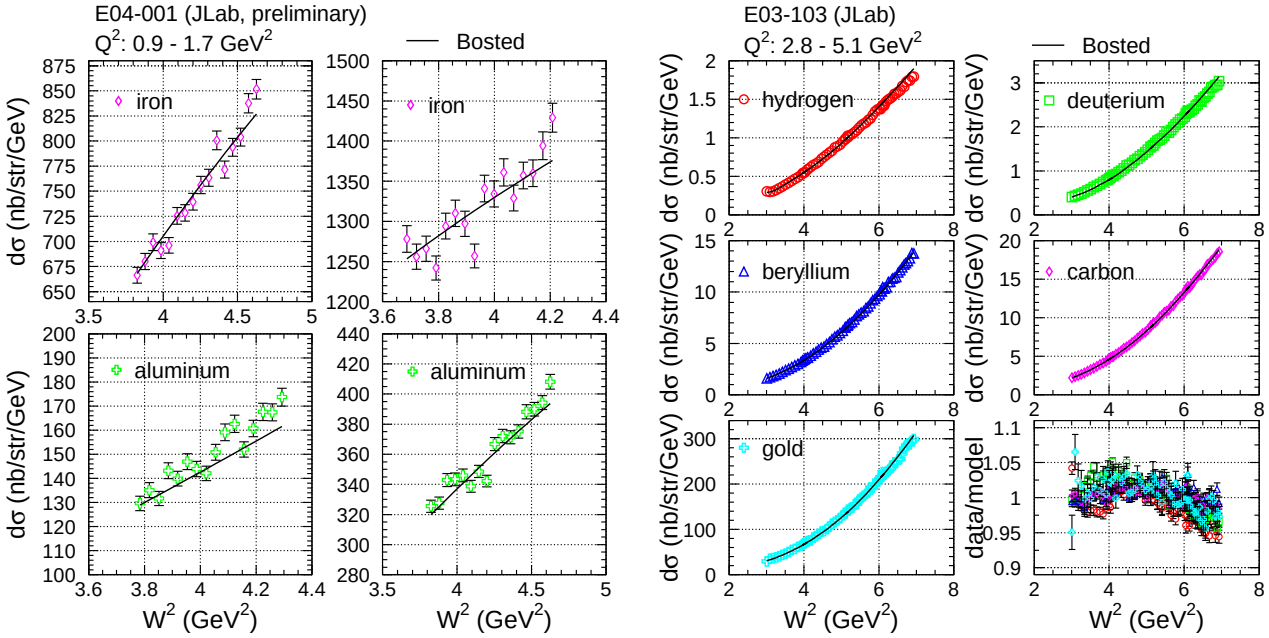

FIG. 15: **Left:** Comparison of P.E. Bosted and V. Mamyan [28] cross section model used for nuclear targets rate calculations to Hall C measurements on iron and aluminum from experiment E04-001 [14]. **Right:** Comparison of the same model to inclusive electron-nucleus cross sections on deuterium, beryllium, carbon, and gold from Hall C experiment E03-103 [29]. Comparisons to data from a hydrogen target are also shown.

x	$I_B(H)$	$R(H)$	$I_B(D)$	$R(D)$	$I_B(C)$	$R(C)$	$I_B(Cu)$	$R(Cu)$	$I_B(Au)$	$R(Au)$
0.100	60	<216	40	<337	30	<386	60	<227	60	<117
0.125	60	<259	40	<370			60	<232		
0.150	60	<388	40	<536	30	<545	60	<336	60	<193
0.175	60	<538	30	<544			60	<449		
0.200	50	<555	25	<559	60	<225	60	<548	60	<34
0.225	60	<294	50	<484			60	<235		
0.250	60	<178	60	<348	60	<463	60	<140	60	<79
0.275	60	<195	60	<380			60	<152		
0.300	60	<199	60	<387	60	<213	60	<154	60	<36
0.400	60	<75	60	<141	60	<38	60	<55	60	<6
0.500	60	<12	60	<22			60	<8		
0.600			60	<3	60	<5	60	<2		

TABLE IV: Beam current, I_B, in μA and total particle rates, R, in kHz for all targets. The rate limits shown include both electron and pion rates. The beam current has been chosen for each kinematic point to keep the detector rates below 600 kHz to ensure good reconstruction of tracks in a high-rate environment. For a fixed x and Q^2 it is important to keep the same beam current for all ϵ points to minimize the associated poin-to-point systematic uncertainties. At low x we are limited by the DAQ rate (3 kHz) so using a larger beam current would not reduce the running time anyway.

of our proposed measurements. There is good agreement between model and measurements for both data sets. We also estimated the rates of pion production in the target using the model of P.E. Bosted [30] based on the fit by Wiser to charged pion production from SLAC [31].

In Table IV we show limits on the electron and pion rates calculated with the models described above for a given beam current for individual x settings. For each fixed central x there could be one or several central Q^2 settings each of those, in turn, corresponding to four or more central beam energy, spectrometer momentum and angle settings (E_B,E_p,θ) as shown in Tables I, II and III. Thus for a given central x we calculated the electron and pion rates for individual (Q^2,E_B,E_p,θ) settings taking into account the spectrometers acceptance (i.e. rates have been integrated over the spectrometers acceptance as indicated in Figure 14) and in Table IV we show an upper rate limit for a given

beam current. Our goal was to keep the raw detector rates below 600 kHz so we used the beam current setting as leverage to control the rate. At high rates the running time will be driven by the data acquisition system rate limit (3 kHz with the 12 GeV Hall C equipment) however it is important to use a beam current setting that limits raw detector rates to values that could be handled without an added ambiguity in the tracking reconstruction and identification in high-rate environments.

C. Backgrounds and Corrections to the Measured Cross Sections

In what follows we will discuss our estimates of contributions from radiative corrections, Coulomb corrections and charge symmetric backgrounds to the cross sections at the proposed kinematics. We will also show our predictions for the pion-to-electron ratios. The magnitude of backgrounds and corrections like the radiated quasielastic contribution to the proposed measurements or the charge symmetric background will be taken into account when estimating the running time to achieve a certain statistical precision. Multiplicative corrections like Coulomb corrections or the inelastic radiative contributions will not affect the **relative** statistical precision but the accuracy in their estimation will affect the overall systematic uncertainty. Where possible we propose additional measurements to ensure a precise knowledge of these corrections.

1. Radiative Corrections

In order to determine the differential cross section that accounts just for the one photon exchange process (the Born cross section), all other contributions from higher order processes in the electromagnetic running coupling constant have to be calculated and corrected for in the measured cross section. Higher order processes include vacuum polarization (the exchanged photon creates particle-antiparticle pairs), vertex processes (a virtual photon is emitted and reabsorbed), Bremsstrahlung emission of real photons, multi-photon exchange. The radiative processes can be divided into two main categories: internal and external. The internal effects take place at the scattering vertex and include internal Bremsstrahlung, vacuum polarization, vertex processes and multiple photon exchange. The external processes (Bremsstrahlung) occur within the target material before or after the primary scattering takes place and are dependent on the target thickness. All the processes described above will lead to energy changes of the incoming and/or the scattered electron.

To obtain the Born inelastic cross section, the radiated elastic/nuclear elastic and quasielastic cross sections are typically subtracted while the inelastic radiative effects are corrected multiplicatively as follows:

$$\sigma_{Born}^{nuclear} = (\sigma_{measured} - \sigma_{elastic\,radiated}^{model} - \sigma_{quasielastic\,radiated}^{model}) * \frac{\sigma_{inelastic\,Born}^{model}}{\sigma_{inelastic\,radiated}^{model}}. \tag{12}$$

For our proposed kinematics the radiated elastic and quasielastic contributions to the total cross section have been calculated using a program based on the formalism by Mo and Tsai [32] that calculates both the internal and external radiative effects. In Figure 16 we show our estimates for 4cm hydrogen and deuterium cryogenic targets and for the 2% r.l. copper and gold solid targets at the central kinematics (red full circles) but also at the kinematics that correspond to the edges of the spectrometers acceptance (green empty circles and blue triangles). For a given scan (E_B,E_p,θ) one acceptance limit is set by the momentum bite of the spectrometer while the other limit by the W^2 cut of 3 GeV^2 (as indicated by the dashed line in Figure 14) since our physics goals focus on the DIS region. We can see that for the kinematic settings at beam energies of 7.7, 8.8 and 11 GeV the correction is well within 10% for all targets while for the lower beam energies within 20%. Thus a 1% uncertainty in the elastic and quasielastic cross section would lead to at most 0.2% uncertainty in the Born inelastic cross section.

x	I_B (μA)	R (KHz)	δ(%)	time (hours)	π/e
0.250	60	<425	0.45	1	<70
0.275	60	<461	0.45	1	<30
0.400	60	<165	0.45	4.5	<160

TABLE V: Beam current, I_B, in μA, detector rates, R, in kHz, projected statistical uncertainty, δ, in % and time estimates for a 6% copper target. The rate limits shown include both electron and pion rates. The time is calculated with the limit of 3 kHz coming from the data acquisition system. The data would be used to verify the accuracy of the external radiative corrections.

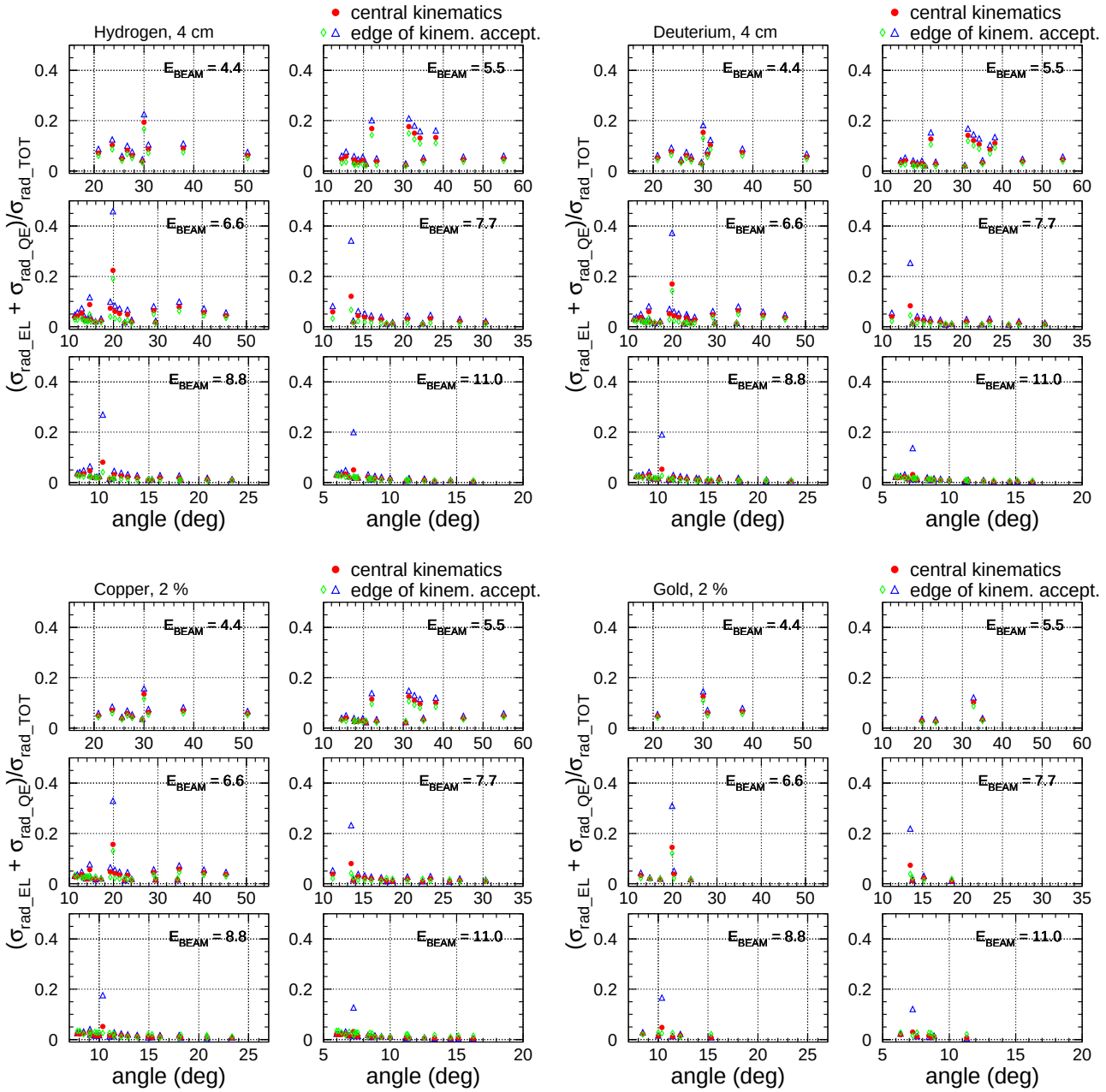

FIG. 16: Estimates of the radiated elastic and quasielastic contributions to the total cross section using the formalism of Mo and Tsai [32] that accounts for external and internal radiative effects. The estimates are shown at the central kinematics (red full circles) but also at the kinematics corresponding to the spectrometers acceptance edges (empty green circles and blue triangles). Some points at the edge of the kinematic acceptance where the correction is large will be discarded. The radiative effects are shown for the cryogenic 4 cm hydrogen and deuterium targets as well as for the 2% r.l. solid targets copper and gold.

The inelastic radiative effects are less sensitive to the ϵ change and therefore have minimal effect on the extraction of R but to set a scale we calculated the total radiative effects at our proposed kinematics and we show our results in Figure 17. In all cases the total radiative corrections will be no larger than 40%. To test our understanding of the external radiative effects we propose to take measurements for a few kinematic points with a 6% r.l. copper target. The magnitude of the external radiative corrections will scale with the radiation length of the target but after accounting for radiative effects the difference in the extracted cross sections, if any, would be a measure of the systematic uncertainty of this correction. We would thus perform the same measurements on a 6% r.l. copper target

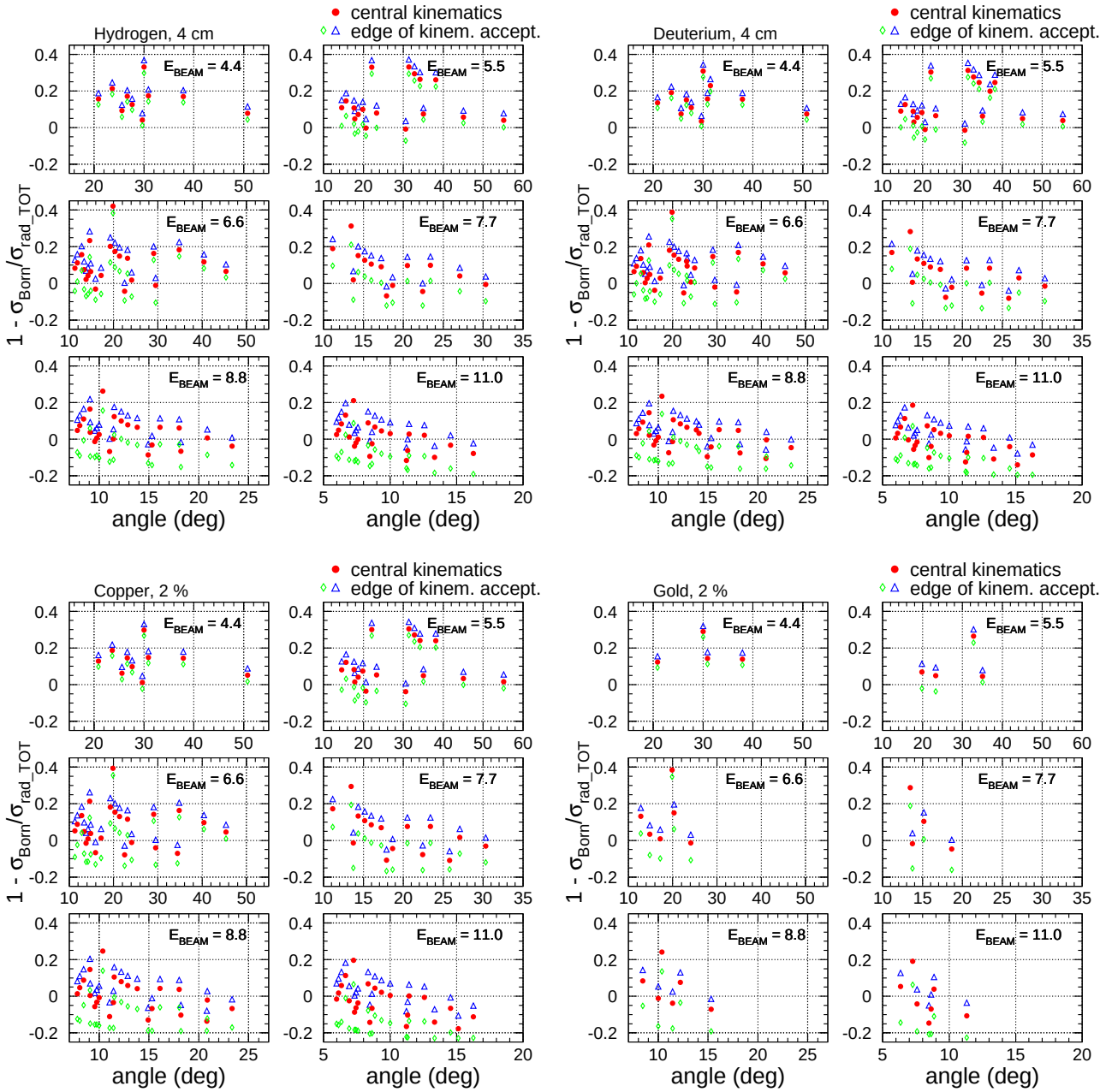

FIG. 17: Estimates of the total radiative effects using the formalism of Mo and Tsai [32] for external and internal radiative effects. The estimates are shown at the central kinematics (red full circles) but also at the kinematics corresponding to the spectrometers acceptance edges (empty green circles and blue triangles). The radiative effects are shown for the cryogenic 4 cm hydrogen and deuterium cryogenic targets as well as for the 2% r.l. solid targets copper and gold.

as with the production 2% r.l. one at x of 0.25, 0.275 and 0.4. Details of these measurements are given in Table V.

2. *Charge-Symmetric Background*

There is a potentially significant probability for neutral pion production in the targets as a result of the interaction with the electron beam. These neutral pions can decay into high energy photons. Another source of photons could be the Bethe-Heitler process. The photons thus produced can further convert into e^+e^- pairs in the target materials or in the materials preceding the detectors contributing to the primary scattered electron yield. This background being

charge-symmetric can be measured directly by changing the polarity of the spectrometers to positive and measuring the produced positrons.

We estimated the possible contribution of the background comming from neutral pion production in the target at all our proposed kinematics and the results are shown in Figure 18 for deuterium and gold. We used the model of P.E. Bosted [30] which employs the fit to the charged pion production data accumulated at SLAC [31]. The neutral pion production is estimated as an average of the positive and negative pion production. The positron cross section is calculated using the decay branching ratios for a neutral pion and the radiation length of the material where a photon that results from the decay can produce e^+e^- pairs. It was found that this model describes fairly well the momentum dependence of the positron cross section for some of the 6 GeV runs [33].

We found that the background contribution to the primary scattered electron yield is no larger than 20%. We plan to measure the charge symmetric background at beam energies of 4.4, 5.5, and 6.6 GeV with few measurements for checks at 7.7, 8.8 and 11 GeV. To estimate the total running time we assume 10% of the production time on each target.

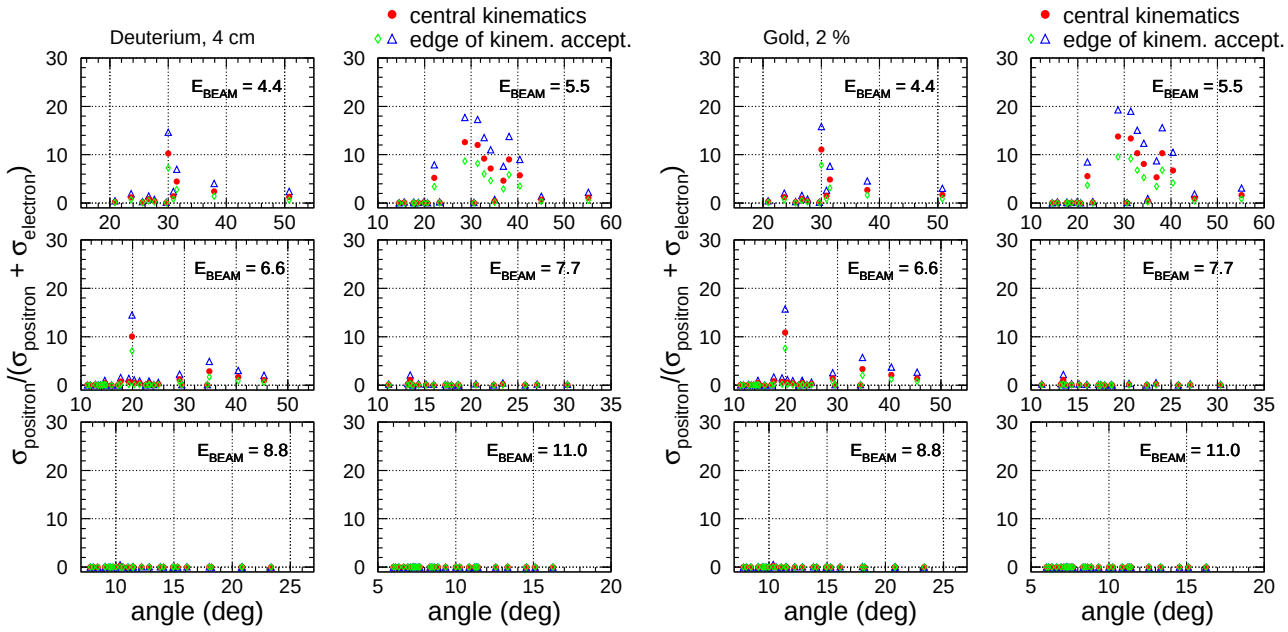

FIG. 18: Charge-symmetric background estimates for deuterium and gold targets for all the proposed kinematics. The calculations are shown at the central kinematics (red full circles) but also at the kinematics corresponding to the spectrometers acceptance edges (empty green circles and blue triangles).For a given scan (E_B,E_p,θ) one acceptance limit is set by the momentum bite of the spectrometer while the other limit by the W^2 cut of 3 GeV^2 (as indicated by the dashed line in Figure 14) since our physics goals focus on the DIS region.

3. *Coulomb Corrections*

Though the Coulomb corrections can be neglected in DIS at very high incident beam energies, for energies in the range of the earlier data from SLAC or at JLab, the Coulomb distortion could result in a non-negligible correction to the cross section. This process refers to the acceleration (deceleration) of the incident (scattered) electrons in the Coulomb field created by nearby protons inside a nucleus via the exchange of soft photons. The net result is a change in the incident and scattered electron kinematics but also a focusing of the electron wave function in the interaction region. Thus the cross sections calculated within the Plane Wave Born Approximation (PWBA) formalism are no longer sufficient and a treatment within the Distorted Wave Born Approximation (DWBA) would be more suitable. However, full DWBA calculations are difficult to implement so typically a more convenient formalism is used: the Effective Momentum Approximation (EMA). In this approximation the incident (E) and scattered (E_p) electron energies are shifted by an average Coulomb potential δE while the focusing factor, $(E + \delta E)/E$ enters quadratically in the cross section calculation. A detailed comparison of the EMA approach and the full DWBA calculation in the quasi-elastic region was performed by Aste and collaborators [34] and it was concluded that the two methodes agree

fairly well. However, the EMA approach has never been tested in the DIS region [13].

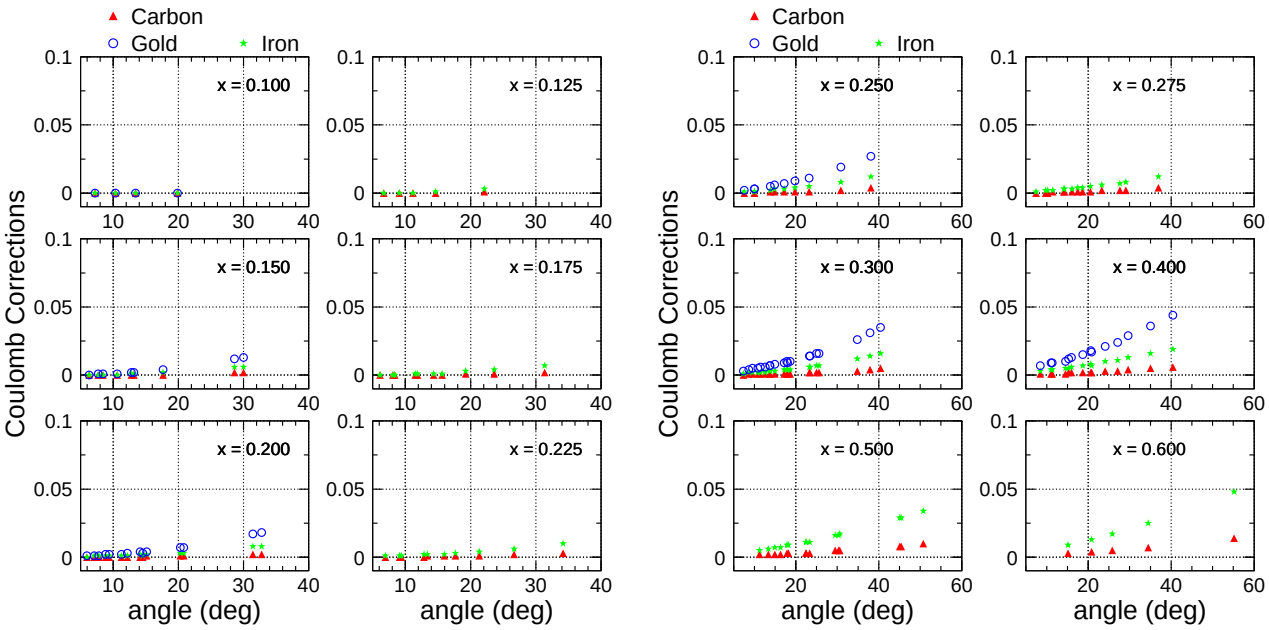

FIG. 19: Coulomb corrections estimated within the EMA framework for carbon, iron and gold targets. Though we will not measure cross sections on an Iron target we show the prediction for the size of Coulomb corrections as these are expected to be similar to those for a copper target.

It would be of much benefit to check the validity of the EMA when applied to Deep Inelastic Scattering in a manner as was done for quasi-elastic scattering. Unfortunately, it has been difficult to interest the theory community in this topic given the lack of relevant precision data. The approval of this experiment should help re-invigorate interest in the application of Coulomb Corrections to DIS. It is worth noting however, that the detailed DWBA calculations performed by Aste [34] resulted in relatively minor adjustments to the "classical" EMA. As it will be shown in what follows, given the relatively small size of the predicted effect for our kinematics, as well as our planned Coulomb Correction test, we expect the systematic uncertainty due to the Coulomb Corrections procedure to to be small.

We calculated the Coulomb corrections within the EMA framework for our proposed central kinematics and the magnitude of the correction is shown in Figure 19 for carbon, iron and gold targets. Though we will not measure cross sections on an Iron target but on a copper one, we show the predicted size of Coulomb corrections as these are expected to be similar to those for a copper target. We see that for a low Z target such as carbon the correction is rather small but for a large Z target (gold) it could reach up to 5% at some of our kinematics. We thus propose to test the EMA approach in the DIS region by measuring ratios of gold to deuterium cross sections at fixed x and ϵ but varying Q^2 as shown in Table VI. The kinematics have been chosen such that for a fixed x and ϵ the Coulomb corrections will vary significantly between the two Q^2 settings. The expectation is that a measured change in the cross section ratio could only be due to the change in Coulomb distortion effects since the nuclear targets to deuterium cross section ratios have been shown to approximately scale with Q^2 [29]. Such a test would require a very good understanding of other corrections and backgrounds. Our calculations of the radiative corrections, the π/e ratio and the charge-symmetric background are shown in Table VII. We would measure the charge symmetric background at the low ϵ setting. We would also take short runs on an aluminum (dummy) target to measure the background comming from the deuterium cryogenic target walls.

4. *Estimates of Pion-to-Electron Ratio*

The π/e ratios have been estimated for all the central kinematics with the model of P.E. Bosted [30] based on Wiser's fit [31] and are shown in Figures 20 and 21. The upper limit on the pion to electron ratio for each target is as follows: for hydrogen the highest ratio is 140, for deuterium 170, for carbon 130, for copper 200 and for gold 120. With a pion rejection factor of 10^{-4}, the contribution of the π^- background to the cross section would be less than 2% for copper and even less for the other targets. At this level the background can be characterized and subtracted

Q^2	x_b	E	E'	θ	ϵ	y	W	C^{Au}_{Coulomb}	R^D (Hz)	Time^D (h)	R^{Au} (Hz)	Time^{Au} (h)
3.48	0.50	4.4	0.69	64.6	0.20	0.84	2.08	11.6%	23.9	1.2	4.1	3.4
9.03	0.50	11.0	1.38	45.5	0.20	0.88	3.10	6.2%	10.5	2.7	1.8	7.8
2.15	0.50	4.4	2.11	27.9	0.70	0.52	1.74	3.5%	1.31k	0.3	223	0.3
5.79	0.50	11.0	4.83	19.0	0.70	0.56	2.58	1.9%	662	0.3	114	0.3

TABLE VI: The event rates, beam time as well as the Coulomb correction for the Coulomb scan test data. Rates assume 60 μA on a 4 cm deuterium cell and a 2% radiation length gold target. Times are for 100k (50k) events for deuterium (gold) at the $\epsilon = 0.2$ settings. We will take short run (0.3 h) with dummy target for deuterium background subtraction.

ϵ	Q^2	Target	*RAD.CORR.*	π/e	Charge-symmetric Background
0.2	3.48	D	1.17	161	0.108
0.2	9.03	D	1.11	106	0.043
0.2	3.48	Au	1.11	6.1	0.180
0.2	9.03	Au	1.09	1.8	0.076
0.7	2.15	D	0.96	6.2	0.0
0.7	5.79	D	0.94	0.6	0.0
0.7	2.15	Au	0.93	1.4	0.0
0.7	5.79	Au	0.91	0.2	0.0

TABLE VII: Backgrounds and radiative corrections factors for Coulomb correction scan settings. Dominant backgrounds are from pion contamination and charge symmetric processes. A 2% gold target has been chosen to minimize (external) radiative corrections and contributions from the charge symmetric backgrounds.

in the offline analysis with good accuracy.

D. Beam-time Request

x	$\delta(H)$	$t(H)$	$\delta(D)$	$t(D)$	$\delta(C)$	$t(C)$	$Q^2(C)$	$\delta(Cu)$	$t(Cu)$	$\delta(Au)$	$t(Au)$	$Q^2(Au)$
0.100	0.5	0.6	0.2	3.3	0.35	1.27	1	0.45	0.73	0.45	0.7	1
0.125	0.5	0.7	0.2	4.1				0.45	0.9			
0.150	0.5	0.6	0.2	3.7	0.35	1.37	1	0.45	0.8	0.45	1	1
0.175	0.5	1.5	0.2	8.7				0.45	1.9			
0.200	0.5	1.6	0.2	9.	0.35	1.7	1.7	0.45	2.	0.45	1.6	1.7
0.225	0.5	1.7	0.2	8.8				0.45	2.2			
0.250	0.5	2.	0.2	9.3	0.35	1.5	1.5	0.45	2.8	0.45	1.2	1.5
0.275	0.5	2.	0.2	8.9				0.45	2.6			
0.300	0.5	3.3	0.35	5.2	0.45	1.1	1.9	0.45	4.8	0.5	1.8	1.9
0.400	0.5	6	0.35	8	0.45	1.2	3	0.45	10.7	0.5	4	3
0.500	0.5	19	0.45	13.5				0.5	31.3			
0.600			0.45	13.3	0.45	10.9	5	0.5	32.9			
total		39		96		19			94		10	

TABLE VIII: Statistical precision goals (δ in %) and the required production running times (t in hours) for hydrogen, deuterium, carbon, copper and gold. The running times are summed up at a fixed x over all Q^2 settings. The total production running time is also shown for each target individually summing over all kinematics. The time estimates shown do not include the aluminum dummy running time.

In Table VIII we show the statistical precision goal (δ in %) and the required production running time for hydrogen, deuterium, carbon, copper, and gold targets. Copper is a heavy enough nucleus to probe nuclear medium effects and we will use it to map in detail both the x and Q^2 dependence of nuclear medium modifications of R, F_1, F_L and F_2. We will perform measurements on carbon and gold at select (x,Q^2) settings in order to determine the A dependence of

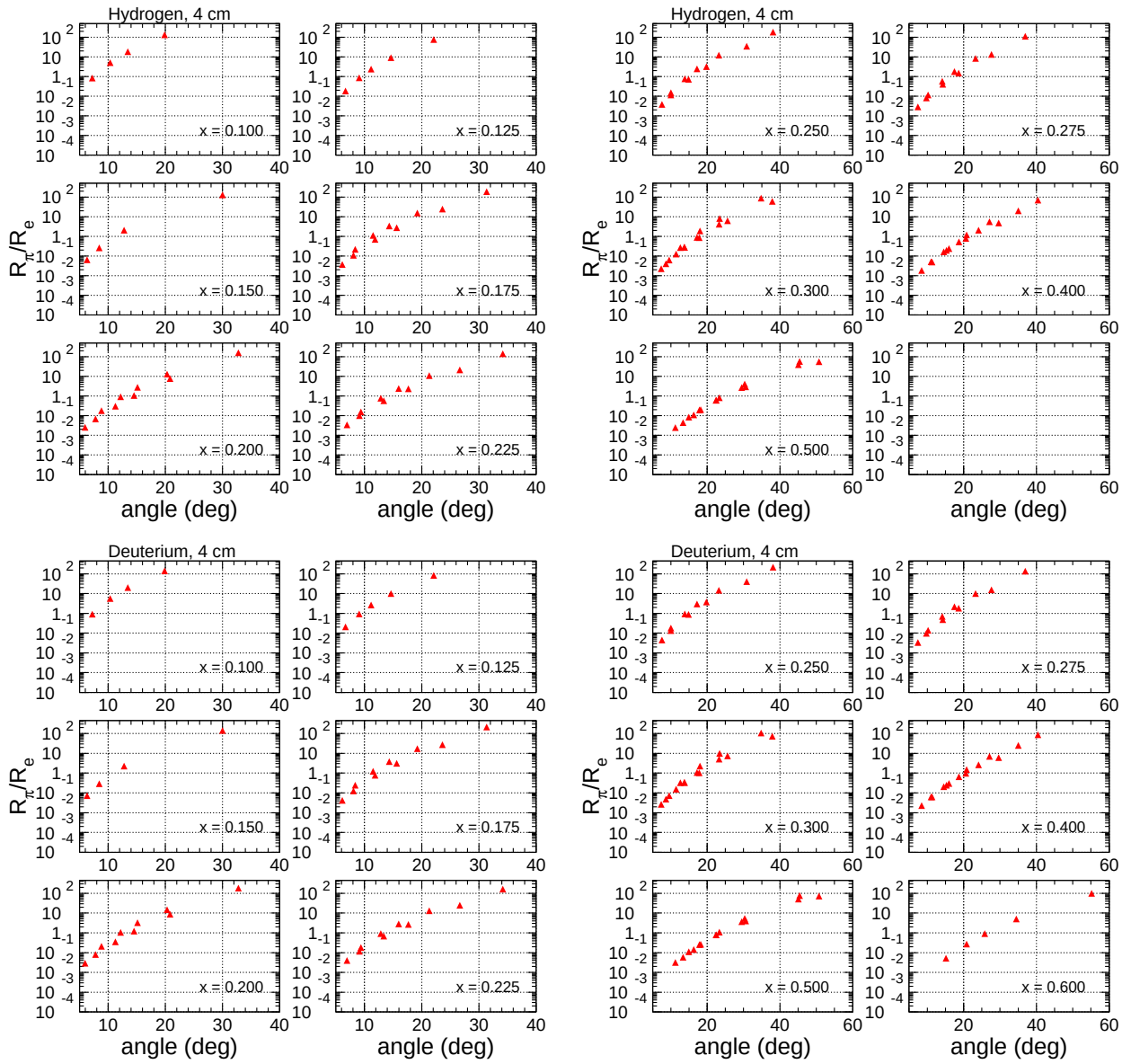

FIG. 20: Pion-to-electron ratios for hydrogen and deuterium.

such effects. The measurements on hydrogen will provide constraints on $R_d - R_p$ and model-independent extractions of F_1, F_L and F_2.

As explained in the Subsection **Kinematics** and as shown in Figure 14, for a given central kinematic setting defined by $(x, Q^2, E_B, E_p, \theta)$ we bin the momentum acceptance of the spetcrometers in bins corresponding to a size in W^2 of 0.1 GeV^2 (in Figure 14 each such bin is shown as an empty circle). The statistical precision shown in Table VIII is targeted for each such individual bin in the kinematic region of $W^2 > 3$ GeV^2. This will allow us to extract the physics quantities with unprecedented statistical precision not only at the central kinematics (indicated by black stars in Figure 14) but also anywhere in the spectrometers acceptance where there is an overlap of at least two or three beam energy settings. Such extractions would require only small Q^2 corrections. The production running times were estimated by assuming an excess of 25% more events than required by our statistical goal in order to account for backgrounds that would be subtracted from the measured cross section and thus would modify the statistical uncertainty (like, for example, the radiated quasielastic contribution, the charge symmetric background or the contribution from the cryogenic target walls).

In Table IX we present our beamtime request. We also show in Appendix A a table with beam time per beam energy where we include the most time consuming experimental activities. We would need a total of 258 hours for

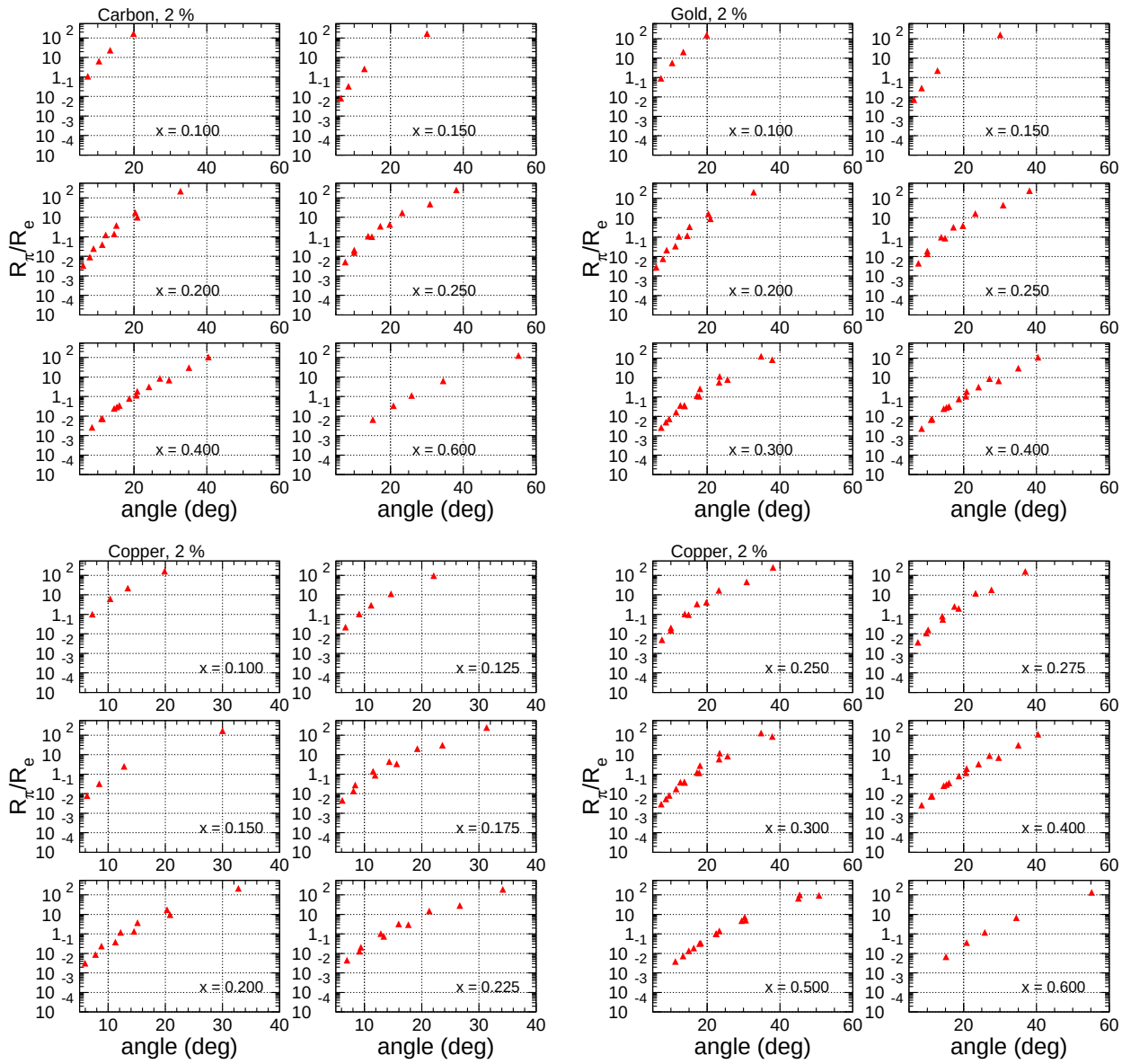

FIG. 21: Pion-to-electron ratios for carbon, copper and gold.

production running on all targets to achieve the statistical precision specified in Table VIII. The external radiative corrections checks and the Coulomb correction scans would require in addition 8 and 20 hours, respectively (please see previous subsections). To measure the background contribution to the hydrogen and deuterium yield coming from the cryogenic target walls we need 15 hours (15% of the total production running time on deuterium). To measure the charge symmetric background we assumed about 10% running time of the production time and this would amount to roughly 26 hours. We estimate that we would need 62 hours for various calibrations of the spectrometers and other equipment. We also plan to measure few momentum scans with both spectrometers where possible for cross-calibration and for that we allocate 6 hours. This type of experiment requires many configuration changes. For beam energy changes we assume a total of 44 hours. We counted 112 momentum and angle changes. We assume that the momentum and the angle of the spectrometers could be changed simultaneously so with an allocated time of 20 minutes per change this would amount to 37 hours. Finally, we will have roughly 506 target changes and assuming 6 minutes per change we would need an additional 51 hours. In total we need 527 hours or 22 days assuming 100% running efficiency.

Category	Activity	Beam Time (Hours)
Production	R, F_1, F_L, F_2 Measurements on H, D, C, Cu, Au	258
Calibrations and Backgrounds	Radiative Corrections Checks	8
	Coulomb Corrections Checks	20
	Cryogenic Traget Walls Background Measurements	15
	Optics (Sieve/Open Collimator; P/θ scan)	24
	Elastic Scattering on H	12
	Beam Energy Measurements (6)	12
	Beam Current Calibration	8
	Horizontal Beam Position Scan on H/D	2
	Target Boiling/Rates Studies	4
	SHMS and HMS cross-calibration	6
	Charge Symmetric Background Measurements	26
Others	Beam Pass Changes	44
	Target Changes	51
	Momentum and Angle Changes	37
Total		527 (22 days)

TABLE IX: Beam time request assuming 100% efficiency.

E. Impact of Proposed Measurements

1. *Measurements on Hydrogen and Deuterium*

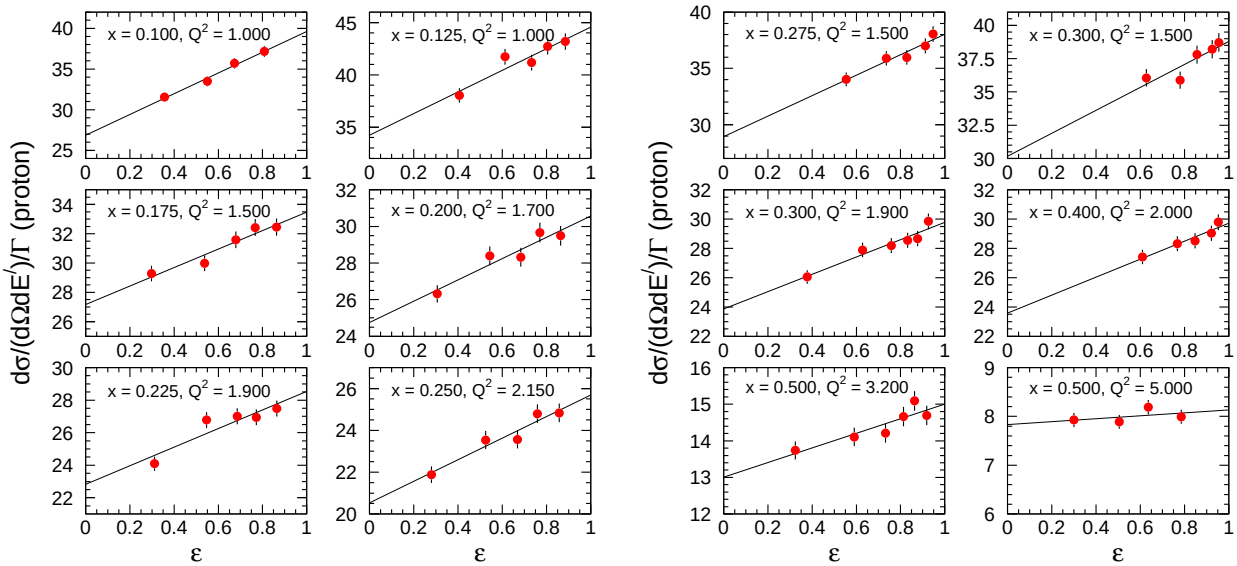

FIG. 22: Examples of L/T separations at fixed (x, Q^2) on a proton target. The ϵ dependence of the radomized reduced cross section $d\sigma/\Gamma$ is fitted and σ_T and R_p and their fit uncertainties are extracted (see text for details). In a given panel we show just one fit example of the many that form the statistical collective at that particular (x, Q^2) kinematics.

In what follows we discuss the impact of our proposed measurements on hydrogen and deuterium targets which will yield R_p, $R_d - R_p$ and a large body of data on the separated proton structure functions F_1, F_L and F_2 in the DIS kinematic region at low to intermediate Q^2. In Figure 22 we show typical fits of the proton reduced cross section $\frac{d^2\sigma}{d\Omega dE'}\frac{1}{\Gamma}$ at some of our proposed kinematics from which σ_T and σ_L are obtained. The reduced cross sections

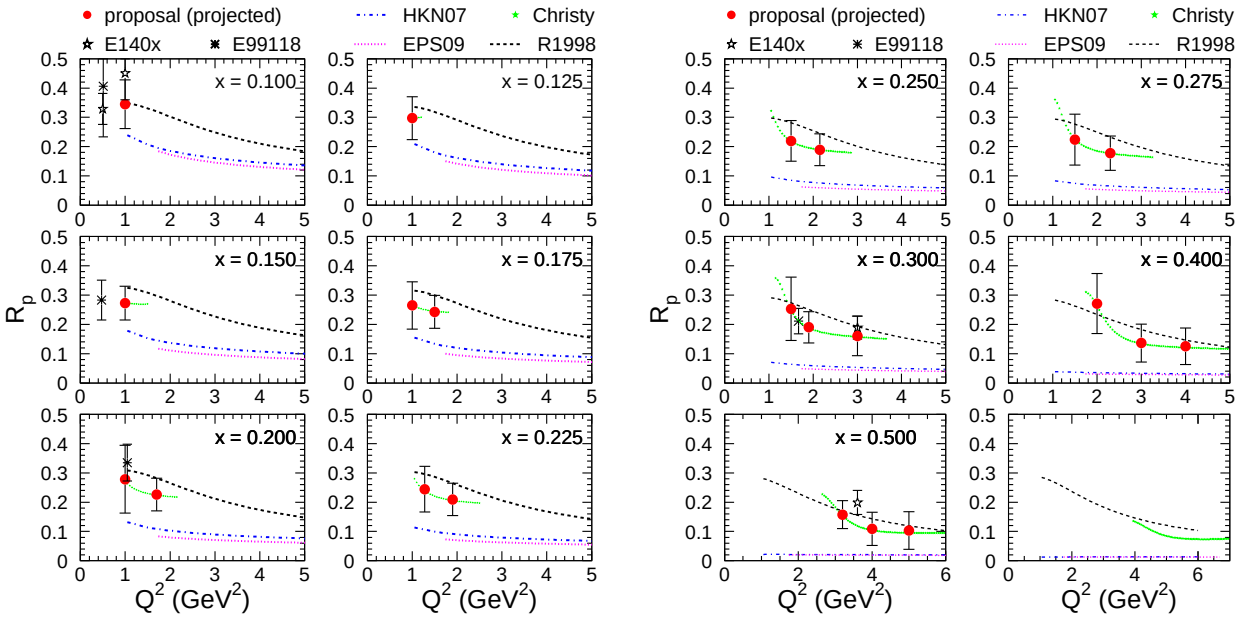

FIG. 23: Projected systematic uncertainties (red circles) in the R_p extraction at all the proposed central kinematics. Parametrizations of R_p from R1998 [37] (black curve), M.E. Christy model [27] (green curve), HKN07 [4] (blue curve) and EPS09 [3] pink curve are also shown. Existing true Rosenbluth LT separations in DIS from SLAC and JLab are displayed in black symbols. For our simulated extractions the model of M.E. Christy has been used as input.

were generated using the model of M.E. Christy [27]. We assumed that we are dominated by systematics and that we can achieve the same systematic accuracy in our extraction of cross sections as the 6 GeV Rosenbluth L/T experiments [35, 36] (a table with the systematics of the 6 GeV experiments can be found in the Appendix B). Thus for the proton reduced cross sections we used a systematic uncertainty of 1.8% and note that we consider this estimate conservative. In order to obtain projections for the uncertainties in the R_p extraction we used the Monte Carlo method to propagate the assumed point-to-point systematic on the reduced cross sections into the extraction of σ_T and R. For this we generate large sets of random numbers that distribute according to a Gaussian with mean of 1 and standard deviation equal to the poin-to-point systematic uncertainty. These are then used as weights for the reduced cross sections. For an extraction of R at a given x and Q^2 such sets are generated and used for each individual reduced cross section point (ϵ point) so that the randomization will yield a Gaussian distribution with a mean equal to the reduced cross section at that particular ϵ point and a standard deviation equal to a value corresponding to a 1.8% relative uncertainty. Then fits are performed to these pseudo-data sets of randomized cross sections with ϵ. In Figure 22, in each panel, just one fit example of the many that form the statistical collective at a particular x and Q^2 is shown. Then σ_T and R and their uncertainties at each (x, Q^2) kinematic point are obtained as the average and the standard deviation of the collective. R_p thus extracted is shown in Figure 23, left panel, and it sits right on the model that was used to generate it, as expected. To estimate the uncertainty coming from using two different spectrometers complementarly for one L/T extraction, we redo the fits varying the HMS reduced randomized cross sections by 1% (we assume that we will cross-calibrate the SHMS and HMS to the 1% precision level). The difference in results is then included in the total uncertainty.

Our projections for the R_p and $R_d - R_p$ measurements are shown in Figures 23, 24 and 25. We will map the dependence of these quantities between 0.1 and 0.5 in x and between 1 and 5 GeV^2 in Q^2. At these particular kinematics very few model-independent Rosenbluth separations exist thus additional experimental constraints on the fundamental quantity R are needed. We show for comparison the data from E140x (SLAC) [6], and from E99-118 (JLab) [7, 36], the only true Rosenbluth L/T extractions on proton currently available in the kinematic range we study. In Figure 23 a fit of R from R1998 [37] and M.E. Christy model [27] are shown together with theoretical calculations (from PDF fits) from HKN07 [4] and EPS09 [3]. The Q^2 dependence of $R_d - R_p$ is of great interest as well: in Figure 25, right panel, we see that existing data show this difference to be negative for $Q^2 < 1.5$ GeV^2 pointing to nuclear medium effects in deuterium of the order of 18 $\pm$ 10% [7] but at higher Q^2 the lack of data precludes any definite conclusions. We would extend these measurements up to a Q^2 of 5 GeV^2.

Our measurements will also produce a large body of data on the separated structure functions F_1, F_L and F_2.

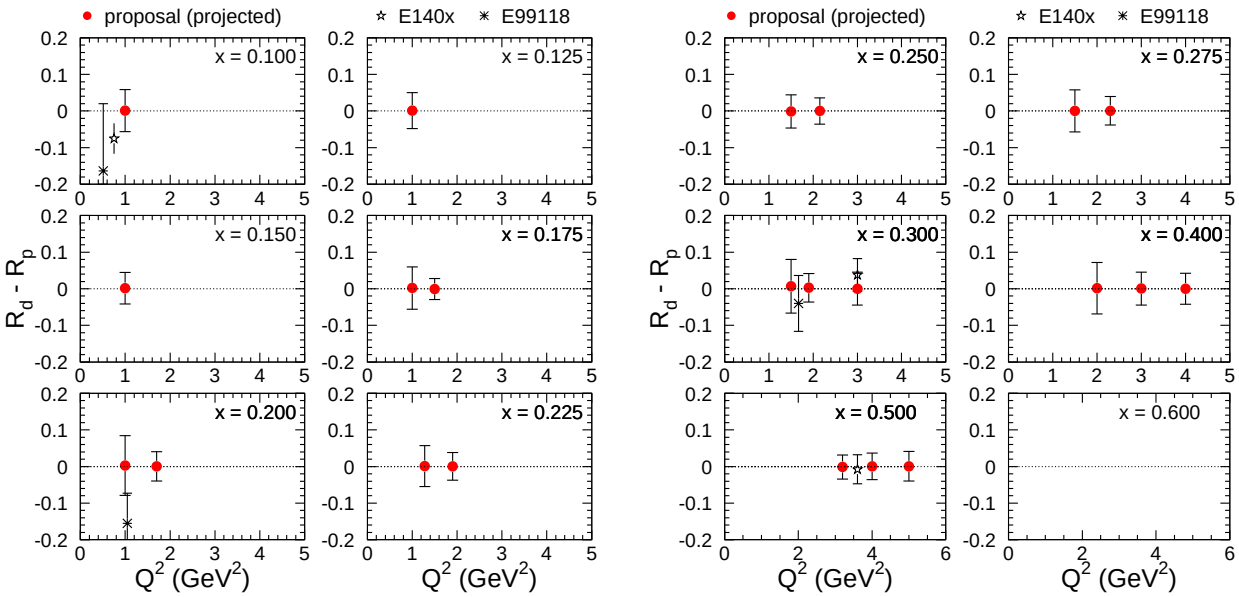

FIG. 24: Projected systematic uncertainties (red circles) for $R_d - R_p$ extractions at all the proposed central kinematics. Existing true Rosenbluth L/T separations in DIS from SLAC and JLab are displayed in black symbols.

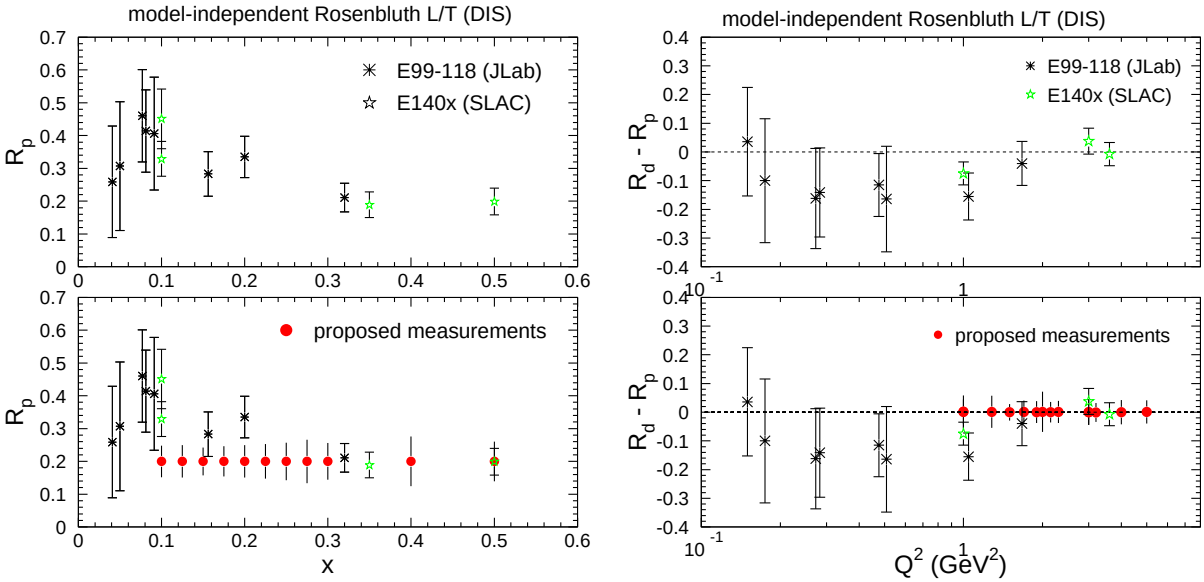

FIG. 25: **Left:** Projected systematic uncertainties on the R_p extraction as a function of x at all proposed central kinematics. **Right:** $R_d - R_p$ versus Q^2: our proposed measurements are shown as red circles while existing data from SLAC and JLab as stars and snowflakes.

Recently, of great interest has been the extraction of moments of the proton F_L structure function [38]. For a pointlike quark the longitudinal structure function F_L is zero but for a composite particle like the proton, F_L is finite and small. Its exact value and momentum dependence reflect the quantum interaction effects between the proton's quarks and gluons. In QCD, one of the features of the proton F_L structure function is its strong sensitivity to the nonperturbative initial state distribution of gluons, $g(x)$. Over the years, due to a lack of F_L measurements, the gluon distribution $g(x)$ has been mostly determined from studying the Q^2 evolution of the F_2 structure function. Just recently [38], given the emergence of more data on the proton F_L structure function from JLab [35] in the resonance

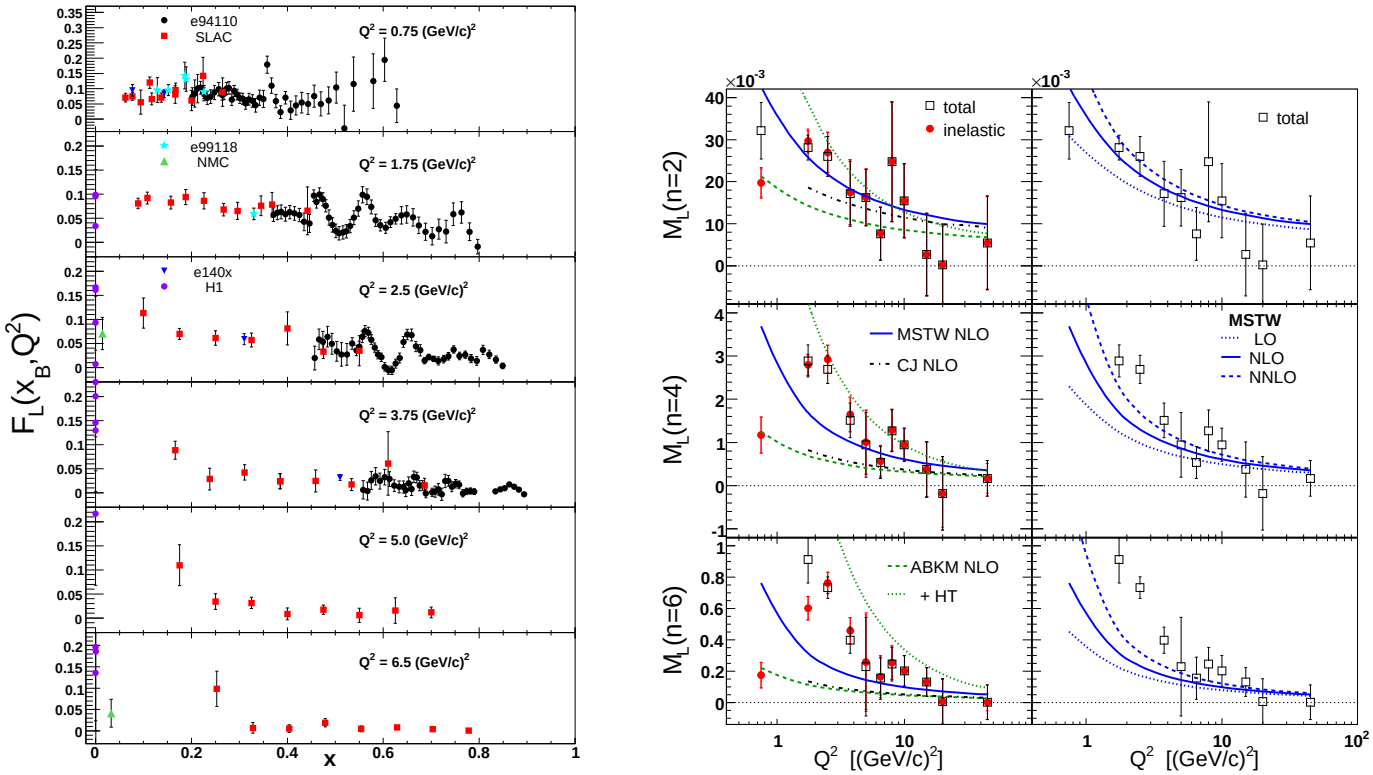

FIG. 26: **Left:** World F_L data on proton for Q^2 between 0.75 and 6 GeV^2. **Right:** Moments of the proton F_L structure function from data compared to moments extracted from state-of-the-art parton distribution functions fits. Figures taken from [38].

region and from HERA [39] in the DIS region at very low x, moments of F_L have been extracted from world data to place additional constraints on existing parton distribution function fits. The world F_L data used in this analysis in the kinematic region of our proposed measurements is shown in Figure 26, left panel while the moment extractions at various Q^2 values and there comparisons to theoretical predictions are displayed in the right panel. Each data point in the right panel in Figure 26 is the result of an integral over the F_L structure function from x of 0 to x of 1 at fixed Q^2. The lack of F_L measurements across the entire x interval at fixed Q^2 is directly reflected in the uncertainties of the moment extractions. The measurements from the JLab experiment E94-110, taken in the resonance region ($W^2 < 3.5$ GeV^2), are shown as black circles in Figure 26, left panel, and they provide the experimental constraints at large x for a given Q^2 up to 3.75 GeV^2. F_L from the model-dependent Rosenbluth extraction by Whitlow *et al.* from SLAC [9] is also shown together with very few data from E140x [6], E99-118 [7], NMC [8] and HERA [39]. Our proposed measurements would cover the DIS region at low to intermediate x, for Q^2 values between 1 and 5 GeV^2. The precision would be very similar to that of the E94-110 data shown as black circles [35].

2. *Measurements on Nuclear Targets*

In Figures 27 and 28 we show our projections for proposed measurements of $R_{Cu} - R_D$. The same procedure as for the proton results was followed to propagate the assumed systematic point-to-point uncertainty of 1.1% on the nuclear targets to deuterium ratios into the extraction of $R_{Cu} - R_D$. We used the model of P.E. Bosted and V. Mamyan [28] to calculate σ_{Cu}/σ_D at our kinematics. The randomized ratios were then fitted with a function given by Equation 11 with σ_T^{Cu}/σ_T^D and $R_{Cu} - R_D$ as fit parameters. The relevant quantity we extract is the uncertainty on $R_{Cu} - R_D$ which connects the projected point-to-point uncertainties on the cross section ratios that we would measure to the physics quantity we would extract.

In Figure 27 we show, besides our projected uncertainties, extractions of $R_{Fe} - R_D$ and of $R_{Au} - R_D$ from the SLAC experiment E140 [2] and an extraction of $R_{Fe+Cu} - R_D$ from re-analyzed SLAC data to include Coulomb corrections by Solvignon and collaborators [13] at $x = 0.5$. Similarly Figure 28 displays the projected uncertainties on

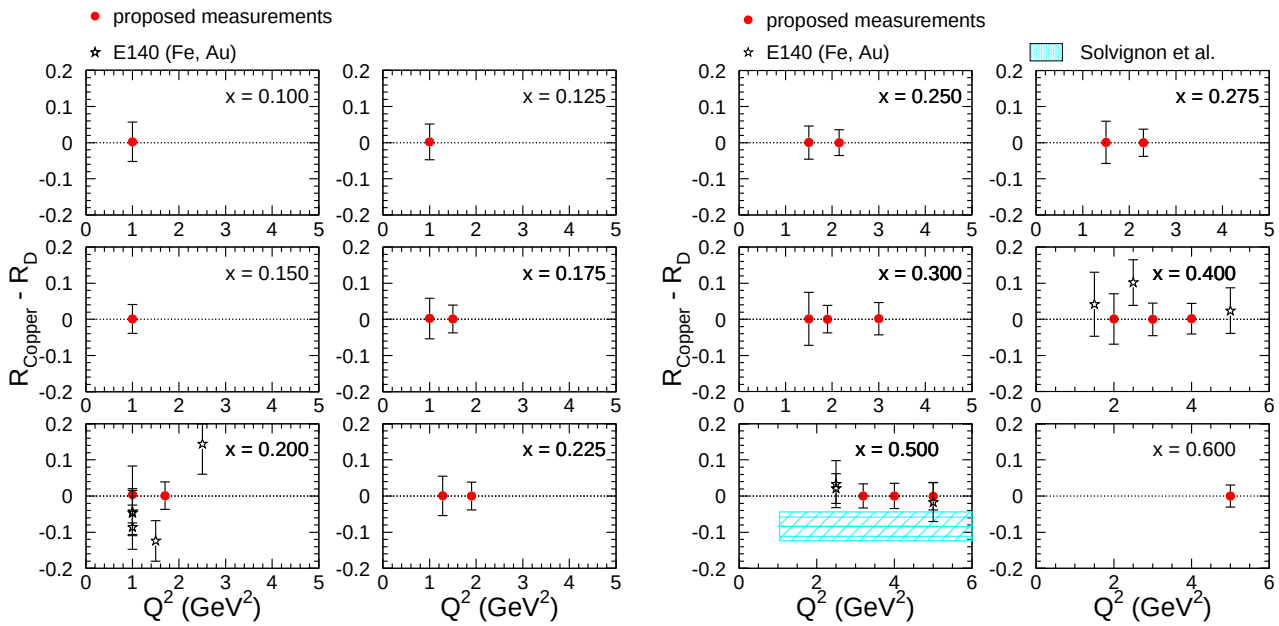

FIG. 27: Projected systematic uncertainties (empty red circles) in the $R_{Cu} - R_D$ extraction at all the proposed central kinematics. Existing true Rosenbluth LT separations in DIS from SLAC E140 are displayed in black symbols. Additionally an extraction of $R_{Fe} - R_D$ and its uncertainty by Solvignon and collaborators [13] from re-analyzed SLAC E140 data to include Coulomb corrections is represented by the cyan band. For our simulated separations the model of P.E. Bosted and V. Mamyan [28] has been used as input. The data points from SLAC shown at x = 0.4 were in fact measured at x = 0.35.

the extraction of $R_{Cu} - R_D$ at all proposed central kinematics as a function of x together with the E140 measurements on iron and gold. It can be seen that our projected uncertainties are comparable or better than those of the few measurements from SLAC with significantly expanded kinematic coverage. We will map the antishadowing region and part of the EMC effect region in great detail in both x and Q^2 with unprecedented accuracy and we will set the most precise limit to date on the possible nuclear dependence of R. Measurements on carbon and gold will also be performed at select kinematics as seen in Table VIII to map the A dependence of nuclear medium modifications of R.

Our proposed measurements will also produce a large set of data on separated nuclear structure functions F_1, F_L and F_2. These can be readily used to test and eventually constrain state-of-the-art extractions of nuclear parton distribution functions. We will also study the nuclear modifications of the nucleon structure in the cross section ratio σ_A/σ_D, as shown in Figure 29. A recent analysis of world data on σ_A/σ_D [40] emphasized the need for additional experimental constraints for copper and gold targets amongst other. In particular, as seen in Figure 29, left panel, there are no published measurements for copper for $x > 0.6$ and the two data points above x of 0.35 have large uncertainties while for gold (right panel) there are no data at low x (the shadowing and antishadowing regions); this precludes a definite confirmation of the universality of the σ_A/σ_D dependence with x. In Figure 29 the published results from EMC and SLAC shown as black squares are displayed together with a fit and its uncertainty, shown as a band, that incorporates both the point-to-point and normalization experimental errors. The width of the band is a measure of the precision and coverage of existing measurements for the cross section ratio. Our proposed measurements shown as red circles with the expected point-to-point uncertainties as bars will map the regions where the cross section ratio is poorly measured. We only show the coverage offered by the proposed central kinematics, however, given the Hall C spectrometers acceptance we will cover both the lower and larger x regions (see Figure 14). We expect a normalization uncertainty on the ratio smaller than 2% for all nuclear targets.

IV. COLLABORATION COMMITMENT TO THE HALL C 12 GEV UPGRADE

The collaboration has a strong commitment to support the equipment for Hall C at 12 GeV. Hampton University played a leading role in the 6 GeV L/T experiments in Hall C, which required many precision systematic studies. These studies led to the detailed understandings of the HMS spectrometer and benefited the Hall C program as a whole. These studies should be repeated for the SHMS spectrometer. Hampton University lead by E. Christy is

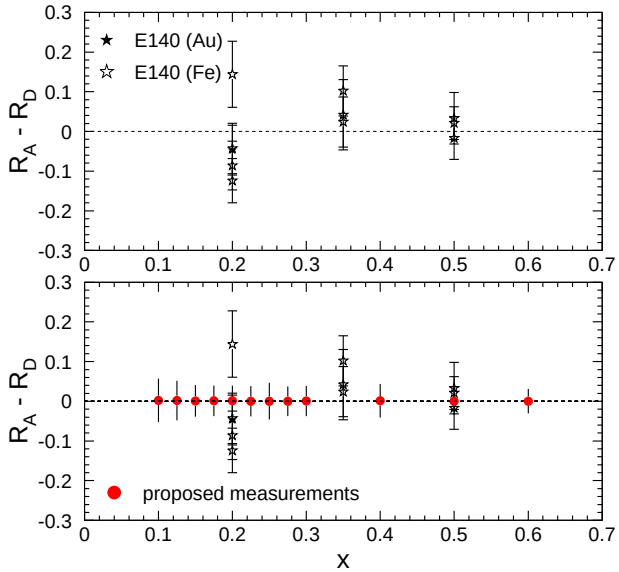

FIG. 28: Projected systematic uncertainties on the $R_{Cu} - R_D$ extraction as a function of x at all proposed central kinematics. Similar extractions at select kinematics (see Table VIII) will be performed for $R_C - R_D$ and $R_{Au} - R_D$. Measurements on iron and gold from SLAC E140 are also shown in black symbols.

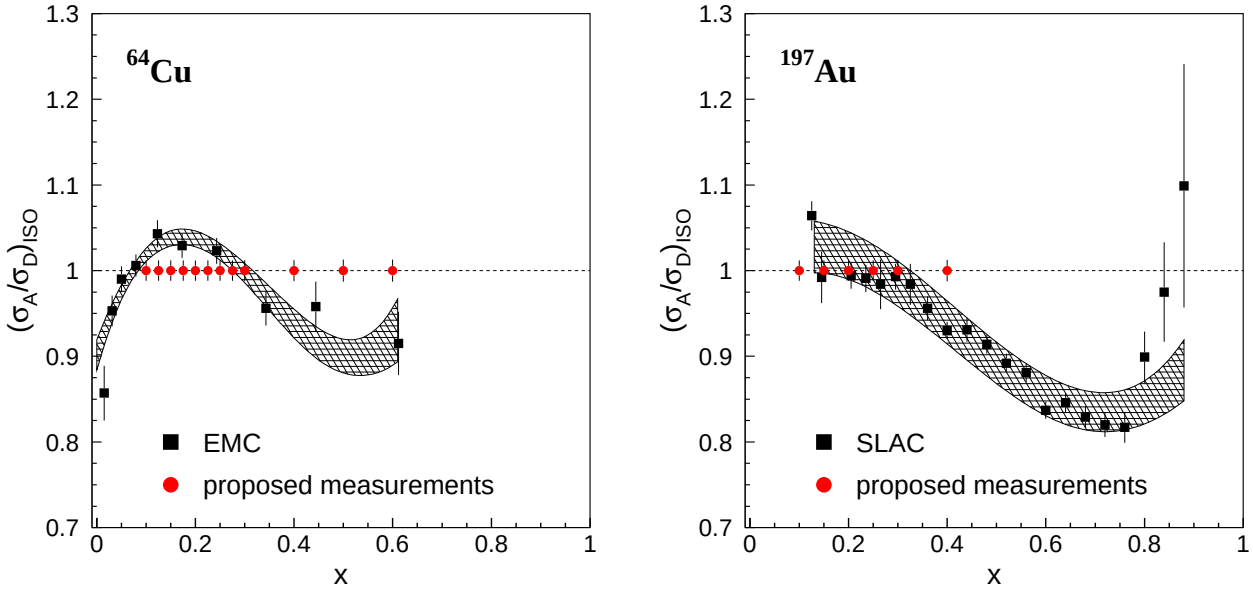

FIG. 29: σ_A/σ_D for copper (left panel) and gold (right pnael). Existing data from EMC and SLAC (black squares) and projections for our proposed measurements (red circles) are shown. We pnly show the coveraged provided by our proposed central kinematics but due to the Hall C spectrometers acceptance we will cover both the lower and larger x regions.

responsible for the construction of the drift chambers for the SHMS spectrometer. The drift chambers construction is in progress. Further commitments include the installation of the chambers into the detector hut and commissioning.

As Hall C staff, David Gaskell will support the SHMS construction and detector assembly and is responsible for ensuring functionality of the Hall C Møller and Compton polarimeters at 12 GeV. He will also update and maintain the Hall C simulation package SIMC, which will help with the spectrometer optics calculations. As Hall C postdoctoral fellow Simona Malace will support the Hall C physics program and participate in hardware tests for the Hall C 12 GeV

upgrade. The James Madison University group lead by I. Niculescu and G. Niculescu are in charge of the construction of the scintillator detectors for SHMS. Alberto Accardi from Hampton University and Vadim Guzey from Petersburg Nuclear Physics Institute will provide theoretical support.

V. SUMMARY

We propose to measure in Hall C at Jefferson Lab with unprecedented statistical precision inclusive inelastic electron-nucleon and electron-nucleus scattering cross sections in the Deep Inelastic Scattering regime spanning a four-momentum transfer range of $1 < Q^2 < 5\ GeV^2$ and a Bjorken x range of $0.1 < x < 0.6$ using hydrogen, deuterium, carbon, copper and gold targets to perform high-precision Rosenbluth separations to extract the ratio $R = \sigma_L/\sigma_T$, $R_d - R_p$, $R_A - R_D$, and the transverse F_1, longitudinal F_L, and F_2 structure functions in a model-independent fashion.

A recently published study looked at implications of a possible nuclear dependence of R for the antishadowing region. It highlighted the lack of true Rosenbluth precision measurements of $R_A - R_D$ and it showed that even a small difference in $R_A - R_D$ currently allowed within the large uncertainties of the available data could have a big impact on the interpretation of the cross section ratio enhancement in the antishadowing region: the effect could be predominantly due to the the longitudinal structure function F_L, instead of F_1 as implicitly assumed in most phenomenological analyses and global nuclear parton distribution fits. Another recent study focused in the EMC effect region re-analyzed SLAC E140 data at $x = 0.5$ including Coulomb corrections and extracted a non-zero value for $R_A - R_D$. That $R_A - R_D$ may be different than zero could have profound implications for our understanding of the origins of both antishadowing and the nucleus EMC effect. The questions above are fundamental, and significant enough that a larger, more precise data set is critically needed. We therefore here ask for 22 days to set the most precise limit to date on the possible nuclear modifications of R. The large body of data that our measurements would produce on separated structure functions for proton and nuclear targets would be used to constrain QCD parton distribution function fits.

VI. APPENDIX A

	4.4 GeV	5.5 GeV	6.6 GeV	7.7 GeV	8.8 GeV	11 GeV
Production	15	71	67	35	35	35
Coulomb correction scan (prod.)	5.2					11.1
E_p, θ changes	3.3	6	7.7	5	7.7	7.7
Target changes	4.6	8	10.4	6.8	10.4	10.4

TABLE X: Time in hours per beam energy for the most time consuming experimental activities.

VII. APPENDIX B

Quantity	Uncertainty	$d\sigma_{DIS}/\sigma_{DIS}$ pt-pt
Beam Energy	0.04%	0.1%
Beam Charge	0.2 μ A	0.5 (*40/I)%
Scattered Electron Energy	0.04%	<0.1 %
Electronic Dead Time	0.25%	0.25%
Computer Dead Time	0.2%	0.2%
Tracking Efficiency	0.3%	0.3%
Detector Efficiency	0.2%	0.2%
Charge Symmetric Background	0.4%	0.4%
Acceptance	0.6%	0.6%
Scattered Electron Angle	0.5 mr	1.0 (*5.5/θ) %
Cryogenic Target Density	0.1%	0.1%
Cryogenic Target length	0.1%	0.1%
Cryogenic Target Background	0.3%	0.3%
Radiative Correction	1%	1% [a]
Total in Cryogenic Rosenbluth Separation	1.8%(1.5% at $\theta > 11.0$)	
Total in Nuclear Rosenbluth Separation	1.7%	
Total in Nuclear/Cryogenic Ratio	1.1%	

[a] It can be bigger for some kinematics.

TABLE XI: Point-to-Point systematic uncertainties in the DIS cross section due to the uncertainty in various experimental quantities. Table adapted from the thesis of V. Tvaskis [36].

[1] M. N. Rosenbluth, Phys. Rev. **79**, 615 (1956).
[2] S. Dasu *et al.*, Phys. Rev. D **49**, 5641 (1994).
[3] K.J. Eskola, H. Paukkunen, C.A. Salgado, JHEP **0904**, 065 (2009).
[4] M. Hirai, S. Kumano, T.-H. Nagai, Phys. Rev. C **76**, 065207 (2007).
[5] D. de Florian and R. Sassot, Phys. Rev. D **69**, 074028 (2004).
[6] L.H. Tao *et al.*, Z. Phys. C **70**, 387 (1996).
[7] V. Tvaskis *et al*, Phys. Rev. Lett. **98**, 142301 (2007).
[8] P. Amaudruz *et al.*, Phys. Lett. B **294**, 120 (1992).
[9] L.W. Whitlow *et al.*, Phys. Lett. B **250**, 193 (1990).
[10] A. Airapetian *et al*, Phys. Lett. B **567**, 339-346 (2003).
[11] M. Arneodo *et al.*, Nucl. Phys. B **481**, 23 (1996).
[12] P. Amaudruz *et al.*, Phys. Lett. B **294**, 120 (1992).

[13] P. Solvignon, D. Gaskell, J. Arrington, arXiv:0906.0512 [nucl-exp] (2009).
[14] V. Mamyan, Ph.D. Thesis, University of Virginia, 2010 (arXiv:1202.1457).
[15] J. Gomez *et al.*, Phys. Rev. D **49**, 4348 (1994).
[16] D.M. Alde *et al.*, Phys. Rev. Lett. **64**, 2479 (1990).
[17] I. Shienbein *et al.*, Phys. Rev. D **77**, 054013 (2008).
[18] A.C. Benvenuti *et al.*, Phys. Lett. B **189**, 483 (1987).
[19] J. Ashman *et al.*, Z. Phys. C **57**, 211 (1993).
[20] Fermi Lab Proposal, http://projects-docdb.fnal.gov/cgi-bin/ShowDocument?docid=395
[21] V. Guzey *et al.*, Phys. Rev. C **86**, 045201 (2012).
[22] S. Dasu *et al.*, Phys. Rev. Lett. **60**, 2591 (1988).
[23] L. B. Weinstein, E. Piasetzky, D. W. Higinbotham, J. Gomez, O. Hen and R. Shneor, Phys. Rev. Lett. **106**, 052301 (2011).
[24] O. Hen, E. Piasetzky and L. B. Weinstein, Phys. Rev. C **85**, 047301 (2012).
[25] J. Arrington, A. Daniel, D. Day, N. Fomin, D. Gaskell and P. Solvignon, Phys. Rev. C **86**, 065204 (2012).
[26] J. Seely *et al.*, Phys. Rev. Lett. **103**, 202301 (2009).
[27] M.E. Christy *et al.*, Phys. Rev. C **81**, 055213 (2010).
[28] P.E. Bosted and V. Mamyan, arXiv:1203.2262 [nucl-th].
[29] A. Daniel, Ph.D. Thesis, University of Huston, 2007.
[30] P.E. Bosted, CLAS-NOTE-2004-005, 2004.
[31] D.E. Wiser, Ph.D. Thesis, University of Wisconsin, 1977.
[32] L.W. Mo, Y.S. Tsai, Rev. Mod. Phys. **41**, 205 (1969).
[33] S.P. Malace, Ph.D. Thesis, Hampton University 2006.
[34] A. Aste, C. von Arx, D. Trautmann, Eur. Phys. J. **A26**, 167-178 (2005).
[35] Y. Liang, Ph.D. Thesis, Amercan University, 2002.
[36] V. Tvaskis, Ph.D. Vrije University, 2004.
[37] K. Abe *et al.*, Phys. Lett. B **452**, 194-200 (1999).
[38] P. Monaghan *et al.*, Phys. Rev. Lett. 110, 152002 (2013).
[39] F. Aaron *et al.*, Eur. Phys. J. C **71**, 1579 (2011).
[40] S.P. Malace *et al.*, arXiv:1405.1270, submitted to the Journal of Modern Physics A.